Optimization of synergistic biosorption of Oxytetracycline and Cadmium from binary mixtures on reed-based-beads: modeling study using Brouers-Sotolongo models

Abstract

The first aim of this study was to synthesize and characterize reed-based-beads (BBR), an enhanced adsorbent from Tunisian-Reed. The second purpose was to evaluate and optimize the BBR efficiency for the simultaneous removal of oxytetracycline (OTC) and Cadmium (Cd(II)), using Central Composite Design under Response Surface methodology. The third goal was to elucidate the biosorption mechanisms taking place. It was shown that under optimum conditions (4.19 g L^{-1} of BBR, 165.54 µmol L^{-1} of OTC, 362.16 µmol L^{-1} of Cd(II), pH of 6, and 25.14 h contact time) the highest adsorption-percentages (63.66 % for OTC and 99.99 % for Cd(II)) were obtained. It was revealed that OTC adsorption mechanism was better described by Brouers-Sotolongo fractal equation, with regression coefficient (R^2) of 0.99876, and a Person's Chisquare (X^2) of 0.01132. The Weibull kinetic equation better explained Cd(II) biosorption (R^2=0.99959 and X^2=0.00194). FTIR and isotherm studies confirmed that the BBR surface was heterogeneous, and that adsorption mechanisms were better described by the Freundlich/Jovanovich equation (R^2=0.99276 and X^2=0.04864) for OTC adsorption, and by the Brouers-Sotolongo model (R^2=0.98510 and X^2=0.77547) for Cd(II) biosorption. Overall results indicate that, at last, the BBR lignocellulosic-biocomposite-beads could be considered as cost-effective and efficient adsorbent, which could be of socioeconomic and environmental relevance.

Introduction

Nowadays, large amounts of medicines (including antibiotics), after being discharged by pharmaceutical industries can be found in the aquatic environment [1]. Antibiotics are also excreted and discharged into water courses as unmetabolized compounds directly within feces and urine [2], thus menacing human beings and ecosystems [3]. In particular, Oxytetracycline (OTC) is an antibiotic very relevant in the treatment of various bacterial infections and animal diseases [4]. Because of its broad antimicrobial activity spectrum, OTC is also widely used as an anti-microbial additive [5,6].

In addition to antibiotics, "heavy metals" are directly and/or indirectly discharged into the environment, by mining operations, metal plating facilities, fertilizer and battery industries,

causing serious environmental pollution [7]. Cadmium (Cd(II)) is considered one of the most hazardous and toxic within these substances. It can cause kidney damage, high blood pressure and destruction of red blood-cells and testicular tissue [8]. Thus, removing this contaminant from water is an urgent task.

Antibiotics and heavy metals are mutagenic and carcinogenic, and not easily biodegradable. Therefore, they present a major danger to the environment and for human beings [3,8]. In addition, OTC and Cd(II) often coexist in soils and wastewater.

Due to the existence of this environmental and public health issue, various biological, physical and chemical techniques have been used to remove these pollutants. Examples of these process are membrane filtration [9–11], coagulation-flocculation [12,13], photocatalytic degradation [14,15], chemical oxidation [16,17], ion exchange [18], electrochemical degradation [12,19], sonocatalytic degradation [20,21], and adsorption [22,23]. Among all of them, adsorption was considered as the most appropriate method to remove pollutants from wastewater, because of its rapidity, simplicity, cost effectiveness, high efficiency, and eco-friendliness [24].

Additionally, there was a wealth of study on the single adsorptive removal of several kinds of contaminants, such as dyes [25], antibiotics [26], and heavy metals [27]. In the case of binary systems, ~~But,~~ most researches focused on the removal of pollutants of the same type However, in spite of the common existence of antibiotics and heavy metals in soils and wastewaters, there is a dearth of works studying their simultaneous removal from binary solution. Specifically, there is a lack of works studying OTC and Cd(II) binary adsorption, when compared with other pollutants.

Furthermore, various adsorbents have been investigated to remove pollutants from wastewater, mainly activated carbon [28], cinnamon soil [29], biomaterials [25,30,31], and many other adsorbents, some of them considered as not highly effective. However, it is not easy to find an efficient adsorbent with potential to retain two different kinds of contaminants at the same time. Therefore, great efforts have been made to produce new adsorbents with high efficiency for binary contaminants removal. This study is the first comprehensive work that assessed the efficacy of Reed-based biocomposite for the simultaneous adsorption of the antibiotic OTC, and the heavy metal Cd(II), from water.

Therefore, this paper reported a two-fold aim. (a) The first objective was to produce a novel, cost-effective and environment-friendly biocomposite beads based on Tunisian Reed (*Phragmites australis*) to be used as an adsorbent. This reed is an invasive plant that flourishes widely in marshes in the Gabes region (Tunisia). (b) The second objective was to evaluate the efficiency and capability of this biosorbent to remove heavy metals (specifically Cd) and antibiotics (specifically OTC) from wastewater simultaneously. (c) The third objective of this study was to evaluate the effect of various biosorption parameters using the CCD (central composite design) methodology. In this regard, compared to traditional single factor testing approaches, the designs approaches are clearly advantageous, because they could be used to model and optimize the effects of various variables with a reduced number of experiments. CCD-RSM (central composite design under response surface methodology) is considered the most efficient methodology to precisely analyze the correlation between dependent and independent variables [32]. It can perform experiments under extreme variables value conditions, guaranteeing accurate results. (d) The fourth goal in this work was to model biosorption kinetics and isotherms data by nonlinear fitting using Brouers-Sotolongo models. The Brouers-Sotolongo kinetic and isotherm models take into consideration the complexity of the biosorption process, and can be used to elucidate the biosorption mechanism. The Brouers-Sotolongo equations have been used in various previous studies [30,33,34], but, to our knowledge, this is the first comprehensive work that has assessed the synergetic CCD optimization of simultaneous antibiotics and heavy metals biosorption and data modelling using Brouers-Sotolongo family equations. In this way, batch biosorption experiments were performed for OTC and Cd(II), to examine the adsorption thermodynamics, kinetics and isotherms data. Finally, possible biosorption mechanisms were also suggested. Overall, the results of these studies could be of relevance as regards treatments to reduce environmental and public health issues related to the simultaneous presence of OTC and Cd(II) in environmental compartments.

Materials and methods

Reagents

Oxytetracycline (OTC, 95 % oxytetracycline hydrochloride ($C_{22}H_{24}N_2O_9HCl$)), and Cadmium (Cd(II), Cadmium nitrate tetrahydrate ($CdN_2O_6.4H_2O$)) were supplied by Sigma-Aldrich (country). In addition, 1-Butyl-3-methylimidazolium chloride (BMIMCl) was purchased from abcr GmbH(country). All mentioned reagents were used without supplementary purification.

Solutions of OTC and Cd(II), at concentrations of 400 µM and 1600 µM, respectively, were prepared and stocked. Afterward, the working solutions were prepared daily by appropriate dilution.

Apparatus

The quantification of OTC in the suspension was carried out on a HPLC liquid chromatograph (Dionex Corporation, Sunnyvale, USA). The injection volume and the flow rate were 50 µL and 1.5 mL min^{-1}, respectively. The mobile phase consisted of acetonitrile (phase A) and 0.02 mol L^{-1} oxalic acid/0.01 mol L^{-1} triethylamine (phase B). The wavelength used for detection of OTC was 360 nm.

The quantification of Cd(II) was carried out using Inductively Coupled Plasma equipped with Optical Emission Spectrometer (ICP-OES) **(**PerKin Elmer Optima 4300 DV, USA).

To designate the functional groups involved in the sorption of OTC and Cd(II) by the BBR beads, infrared spectra were obtained for the biosorbent, before and after contact with OTC and Cd(II) pollutants, using a Fourier Transform Infrared Spectrophotometer equipped with Attenuated Total Reflection Method (FTIR-ATR, PerkinElmer, USA). The baseline correction related to the atmospheric air was repeated for each sample. The spectral resolution was 2 cm^{-1} and four scans were realized for each sample, with 450-4000 wave-numbers range. To observe the surface morphology of biosorbent, a scanning electron microscope (SEM) equipped with energy dispersive X-ray (EDX) (ESEM EVO LS15, Zeiss, Germany) was used. SEM-EDX allows quantifying the surface chemical composition before and after sorption.

Thermo-gravimetric measurement of BBR was performed using thermogravimetric analyzer (TGA, 4000 PerkinElmer, USA), under N_2 atmosphere, with heating rate of 10 °C min^{-1}, to determine the BBR thermal stability. The sample was heated from 30 to 900 °C. The amount of the BBR sample was about 4.813 mg.

The specific surface area of BBR was determined using the N_2-BET (Nitrogen-Brunauer-Emmett-Teller) adsorption test (Micrometrics Instrument Corp., USA).

Bio-sorbent preparation

The biocomposite beads of Reed (referred to as BBR) were synthesized using the Karoui et al.'s protocol [30], as follows: The Tunisien reed (R) was cleaned, dried and sieved to obtain the reed powder. In the present work the used biosorbent is composed of regenerated Tunisien reed (RTR) and charcoal of Tunisien reed (ChTR) with equal quantities. On the one hand,

after treated the reed powder with the orthophosphoric acid (H_3PO_4) solution (1M), the obtained mixture was neutralized until pH = 6.95 ± 0.5, and the powder was carbonized at 250 °C to obtain the ChTR. On the other hand, the reed was dissolved in BMIMCl, and then the ChTR was added [30]. Afterwards, the viscous and homogeny mixture was added drop-wise into a distilled water bath using pipette with a diameter of 3 mm.

, In a further step, the obtained beads were thoroughly rinsed with distilled water until disappearance of BMIMCl (control realized by electric conductivity and pH measurements). Finally, the BBR were frozen at T = -17 °C, to prepare it for lyophilization. The formed beads were stocked in desiccators before other use.

Adsorption Experiments

Batch binary biosorption experiments were carried out in 50 mL glass bottles. All solutions were stirred at 150 rpm by the mean of horizontal shaker at room temperature. The central composite design (CCD) methodology was used to obtain the optimum sorption conditions and to study the effect of various factors on pollutants removal efficiency. Then, the temperatures (20–50±1°C) were chosen to perform and discuss the thermodynamic study for OTC and Cd(II) binary sorption onto BBR beads.

Percentage removal (%R) and the adsorbed amount q_e at equilibrium were determined using Eq(1) and Eq(2), respectively [35]:

$$q_e = (C_0 - C_e)V/m \quad (1)$$

$$\% R = 100(C_0 - C_e)/C_0 \quad (2)$$

Where, C_0 and C_e are the initial and the equilibrium concentrations (mg L^{-1}), respectively; V is the solution volume (L); m is the mass of biosorbent (g).

Error analysis

To designate the best kinetic or isotherm equation applicable in the current study, non-linear correlation coefficients (R^2), chi-square test (χ^2), and residual sum of squares (RSS) were evaluated as alternatives for informing on the sorption process. **Table 1** shows the used equations to calculate the R^2, χ^2 and RSS values.

Table 1.

Experimental design and statistical treatment

STATISTICA12.0 software was used to analyze the experimental data, obtained by central composite design under response surface methodology (CCD-RSM). Both OTC and Cd(II) removals were determined by using batch-type binary adsorption experiments. The CCD-RSM methodology was used to optimize the experimental conditions and minimize the number of experiments [30]. The effect of all tested parameters and the interactions among the controlled factors on the biosorption percentage were evaluated using CCD. [36]

In this paper, five factors including the adsorbent dosage (F_1: 2 – 4 g L^{-1}), the OTC concentration (F_2: 175-275 µmol L^{-1}), the Cd(II) concentration (F_3: 400-800 µmol L^{-1}), the pH (F_4: 4-8) and the reaction time (F_5: 12-24 hours), were evaluated to determine the optimum sorption conditions. The used low values of adsorbent dosage were chosen to save biomaterials. In addition, taking into account that the concentrations of antibiotic and heavy metal detected in wastewater were low, narrow ranges of OTC and Cd(II) concentrations were chosen. The experimental design was performed in a large range of pH (acid and basic media). Some preliminary tests showed that the OTC and the Cd(II) biosorption process onto BBR was slow. Therefore, the time range estimated in this work was 12-24 h. A number of 47 experiments were carried out under non-factorial central composite rotatability design. This number is the sum of 5 center points (replicates), 10 axial (star) points, and 32 factorial (cube) points. Each factor was coded at 5 levels, which are the lowest (-α), low (-1), the center point (0), high (+1) and the highest (+α) levels.

Table 2 represents the value corresponding to each level for both OTC and Cd(II) contaminants.

Table 2.

For a central rotatable composite design, the axial distance α (distance between the star point and the design center) was expressed by Eq. (6):

$$\boldsymbol{\alpha} = [n_c]^{\frac{1}{4}} \qquad (6)$$

where n_c stands for the number of cube points in the design.

The developed empirical model to correlate the response (adsorption percentage) to the five studied independent variables was given by the following mathematical relation (Eq. (7)), which is based on second-order quadratic model.

$$Y = b_0 + \sum_{i=1}^{k} b_i F_i + \sum_{i=1}^{k} b_{ii} F_i F_i + \sum_{i=1}^{k} \sum_{j=i+1}^{k} b_{ij} F_i F_j \quad (7)$$

Where, Y is the predicted dependent variable (predicted adsorption percentage); b_0 is the model constant; b_i is the linear coefficient; b_{ij} is the squared (quadratic) coefficient; b_{ij} is the cross-product coefficient; and F_i, F_j are the independent variables.

The experimental design points and the findings for binary antibiotic and heavy metal adsorption were illustrated in **Table S1**. The five central points show the experimental data reproducibility.

Table S1 (Supplementary Material)

Kinetic models

OriginPro 8.5 software for Windows was used to carry out processing of the non-linear data and the derivatives spectra. The kinetics Brouers-Sotolongo family model, based on the BurrXII statistical distribution [37], was the most developed fractal theory applied to study the kinetics sorption of pollutants onto porous adsorbents [38].The statistical macroscopic kinetic model BSf (n,α) widely integrates irreversibility, fractal adsorption and diffusion, and the sorption-desorption mechanism nature of the process [30].

The BSf (n,α) was expressed by Eq (8) and Eq (9) (**Table. 3**). Five approximate models can be obtained from the general BSf model (n,α) by giving well-defined values to n and α. The five equations are indicated in **Table. 3.**

Table 3.

In this work, the adsorption kinetic results of the OTC and Cd(II) uptake onto BBR were depicted using Brouers-Sotolongo-fractal BSf equation (n, α), as was described in various previous papers [30,33,34]. The pseudo-first-order model (PFO; n = 1 and α = 1), the pseudo-second-order model (PSO; n = 2 and α = 1), the Weibull kinetic (n =1 and α ≠ 1), the Hill kinetic (n = 2 and α ≠ 1), and the Brouers-Gaspard kinetic (BG; n = 1.5) were employed to study the binary biosorption of organic and inorganic substances onto the BBR in liquid phase and to analyze the experimental data obtained.

Adsorption isotherms

The equilibrium adsorption isotherm is based on the relation between the equilibrium concentration in the liquid-phase (Ce) and the amount adsorbed at equilibrium per unit of mass (q_e) [25].

The General-Brouers-Sotolongo (GBS) equation is expressed by Eq (15) and Eq (16) (**Table. 4**), and $C_{e_{\frac{1}{2}}}$(50 % of *Ce*), that depends on the "a", "b" and "c" constants, was calculated using Eq (17) (**Table. 4**). Six approximate models can be obtained from the GBS equation by giving well-defined values to "a" and "c" parameters. The six equations are indicated in **Table. 4.**

Table 4.

In this work, the GBS, the normal Brouers-Sotolongo (BS; c = 0), the Freundlich (c = 0 and $C_e \ll b$), the Jovanovich (c = 0 and a = 1), the Hill-Sips (HS; c = 1), the Langmuir (c = 1 and a = 1) and the Brouers-Gaspard (BG; c = 0.5) isotherms were used to analyze adsorption data and describe the interaction between the BBR adsorbent and the OTC and Cd(II) adsorbates.

The experimental conditions used in the kinetic and isotherm studies are the optimal adsorption conditions obtained by the CCD-RSM design. The consistency between the experimental and the predicted values was assessed using the coefficients of correlation (R^2). Moreover, the kinetic and isotherm equations appropriateness was verified by the reduced Chi-square (χ^2) and the residual sum of square (RSS).

Results and discussion

Biosorbent Characterization

The determination of pH_{pzc} was performed to examine the relationship between the adsorbent surface charge and the solution pH. NaOH and HCl solutions were used to adjust the pH of 0.01M NaCl solutions, in the range 1-12. Then 50 mL of NaCl at each pH and 0.15 g of BBR biosorbent were mixed for 24 h and stirred at 350 rpm. Then, the pH_{final} of each solution was measured using an Orion Star A211 pHmeter (Thermo Fisher Scientific, USA) [39]**.**

The pH_{pzc} value corresponds to the intersection of the bisector line and the graphical representation of pH_f versus pH_i.

The pH_{pzc} value of BBR adsorbent was found to be 4.7, as indicated in **Fig. 1.** At pH < pH_{pzc}, the biosorbent surface is positively charged, and the biosorption of anions is favored. Whereas, at pH > pH_{pzc}, the biosorbent surface is negatively charged, and biosorption of cations is favored [40,41].

Fig. 1.

Fig. 2. exhibits the FTIR-ATR spectra for the BBR particles, before and after adsorption of OTC and Cd(II). The spectra of BBR revealed the presence of the characteristic functional groups of lingo-cellulosic material. In line with Karoui et al. [30], the O-H and C-H stretching medium band between 3650 and 3000 cm^{-1} can be related to the presence of cellulose and hydrogen bonds association. Peaks at 2918 and 2850 cm^{-1}, attributed to C–H bonds, were observed on the BBR and BBR-OTC-Cd(II) spectra. As was reported by Alshaheri et al. and Guedidi et al. [42,43], the peak at 1713 cm^{-1} on the BBR and BBR-OTC-Cd(II) spectra is related to the CO_2 and C=O elongation vibration obtained from the transformation of phenols, ketones, esters, ether and/or aromatic carboxylic groups. As was previously explained by Guedidiet et al., Song et al., and Karoui et al. [30,43,44], the vibrations at 1595 and 1600 cm^{-1} could be ascribed to C=C of aromatic vibrations, asymmetric COO^-, and/or the C=O conjugated with aromatic bonds. These signals would indicate the presence of lignin [45]. In line with Taylor et al. [46], the peak observed at 1234 cm^{-1} could be related to the C-H, C–O, and C-O-H bonds in carboxylic acids. The peak, present in BBR spectra, near 1039 cm^{-1} originating from carbonyl peak can be ascribed to the cellulose structure. The BBR spectra before and after bisorption showed a peak at 897 cm^{-1}, assigned to C-C band. As observed, OTC and Cd(II) adsorption showed H-C-H peak appearance at 1317 cm^{-1} [47].This finding indicates the OTC antibiotic adsorption on the BBR surface. After binary biosorption onto the BBR surface, the band at 1039 cm^{-1}, attributed to the C=O bond, moved to 1034 cm^{-1}. This shift confirmed that direct complexation between OTC and the BBR functional groups could be occurred. In the same way, the band at 1595 cm^{-1} related to the C=C of aromatic vibrations shifted to 1588 cm^{-1}. These shifts should be due to the biosorption phenomena. Furthermore, the presence of Cu(II), simultaneously to OTC, lead to slight shifts of wave-numbers from 1600 to 1609 cm^{-1} and from 1595 to 1588 cm^{-1} in the C=C , COO^-, and C=O peaks [48], and enhancement in the intensity of carboxylic acids bonds at 1234 cm^{-1} and C-C deformation at 1370 cm^{-1}. Finally, after OTC and Cd(II) adsorption, a decrease in the intensity of the CO_2 and C=O bands at 1713 cm^{-1} and a phenyl vibration band at 740 cm^{-1} were observed [49]. These changes suggested that the carbonyl and phenolic groups of BBR reacted with Cd(II) to form inner-sphere surface complexes, thus generating BBR-O≡Cd-OTC ternary complexes [44].

In summary, the appearance of new characteristic groups for OTC and Cd(II), the increase/decrease of the intensity of some bands and the shifts of other peaks would confirm the adsorption of OTC and Cd(II) pollutants onto the BBR particles.

Fig. 2.

The SEM micrographs of BBR before the simultaneous adsorption of OTC and Cd(II) are shown in **Fig. 3**. In fact, **Fig. 3a1**, **a2** illustrate a porous adsorbent morphology with cavities of different sizes and shapes. Similarly, the SEM images of BBR exhibit an irregular surface and uneven structure. On the basis of these characteristics, it can be deduced that the BBR biosorbent has a suitable morphology for biosorption process. **Fig. 3b1, b2** represent SEM micrographs of BBR loaded OTC and Cd(II). It is observed that the surface porosity of BBR decreased after binary biosorption phenomena due to reaction of OTC and Cd(II) with the active sites of BBR. Therefore, after adsorption, the BBR surface became more regular and smoother compared to BBR surface morphology before adsorption, indicating filling of BBR surface by OTC and Cd(II) molecules.

Fig. 3

Thermogravimetric (TGA) curve of BBR beads was also investigated (**Fig. S1**). The first step of weight loss (about 5.2 % in the range of 35-100 °C) is assigned to dehydration. The major charring occurred in the range of 370-220 °C, with weight loss of 61.48 %, and was observed for BBR adsorbent, considering that it was mainly caused by the hemicelluloses depolymerization, the cellulose glycosidic bonds breakdown, and the lignin decomposition, as previously interpreted by Karoui et al. and Ben Arfi et al. [30,50].

Fig. S1 (Supplementary Material)

Surface area and porosity parameters were obtained using nitrogen (N_2) adsorption at temperature of 77 K. The N_2 adsorption/desorption isotherms for BBR beads are shown in **Fig. S2**. BET surface area, pore diameter and total pore volume of BBR adsorbent were found to be 9.1 ± 0.1 $m^2\ g^{-1}$, 9.7 ± 0.1 nm and 21.5 ± 0.1 $mm^3\ g^{-1}$, respectively. The surface area value of BBR confirms previous findings reported by Montanher et al. and Mohan et al. [51,52], which revealed that biomass-materials are often characterized by low surface area values. Moreover, the BBR average pore size was in the range of 2–50 nm, indicating the presence of mesopores.

Fig. S2 (Supplementary Material)

Statistical analysis

The results of the CCD analysis led to the following second-order-polynomial equations:

$$Y_{(\%R\ OTC)} = 50.11 + 10.96F_1 - 6.81F_2 + 0.93F_3 + 0.21F_4 + 4.63F_5 - 3.25F_1^2 - 2.94F_2^2 - 0.09F_3^2 - 4.13F_4^2 - 1.31F_5^2 + 0.64F_1F_2 - 0.026F_1F_3 - 0.64X_1F_4 - 1.33F_1F_5 - 0.19F_2F_3 - 3.13F_2F_4 - 0.08F_2F_5 + 1.60F_3F_4 + 0.10F_3F_5 - 0.41F_4F_5 \quad (23)$$

$$Y_{(\%R\ Cd(II))} = 74.36 + 6.49F_1 + 1.84F_2 - 9.78F_3 + 17.88F_4 + 1.98F_5 - 1.13F_1^2 + 1.09F_2^2 - 2.79F_3^2 - 2.41F_4^2 + 0.52F_5^2 - 0.07F_1F_2 + 0.7F_1F_3 - 3.77F_1F_4 - 0.85F_1F_5 + 0.77F_2F_3 + 1.60F_2F_4 - 0.05F_2F_5 + 2.02F_3F_4 + 0.21F_3F_5 - 0.92F_4F_5 \quad (24)$$

Positive coefficients in these equations indicate favorable effects on the adsorption of the pollutants. Conversely, negative coefficients indicate unfavorable effects on the adsorption of the antibiotic and heavy metal from binary aqueous solution.

Table S2 illustrates the ANOVA results for the response surface quadratic model corresponding to OTC and Cd(II) removal. The correlated model relevance was assessed using the Fisher value (F-value) for each factor at a confidence interval of 95%. The factor significance was evaluated by the probability value (p-value). In fact, a factor with p-value less than 0.05 is significant in the statistical model. Whereas, a factor with p-value high than 0.05 is not statistically significant, and thus can be considered ignorable.

Table S2. (Supplementary Material)

The Pareto graphs of OTC and Cd(II) **(Fig. S3)** were also used to describe the significance of the factors in the statistical models. As can be seen in **Fig. S3.a** the adsorbent dosage was the most important independent variable for OTC removal. Besides, the OTC concentration, the contact time, the quadratic pH factor, the quadratic adsorbent dosage, and the interaction of OTC concentration and pH, were also found to be significant factors for OTC removal from binary system. Similarly, **Fig. S3.b** shows that pH was the most important parameter for Cd(II) removal. This result confirms that pH is the most important operating parameter. In addition, the Cd(II) concentration, the adsorbent mass, the interaction of adsorbent mass and pH, the quadratic Cd(II) concentration, the quadratic pH, the reaction time, the OTC concentration and the interaction of the Cd(II) concentration and pH had significant impact.

Fig. S3 (Supplementary Material)

ANOVA analysis (**Table S2**) and Pareto charts **(Fig. S3)** were reported to keep the significant terms and eliminate the insignificant terms. Thus, the correlated models of OTC and Cd(II) removal efficiencies can be described by the following equations:

$$Y_{(\%R\ OTC)} = 50.11 + 10.96F_1 - 6.81F_2 + 4.63F_5 - 3.25F_1^2 - 2.94F_2^2 - 4.13F_4^2 - 3.13F_2F_4 \quad (25)$$

$$Y_{(\%R\ Cd(II))} = 74.36 + 6.49F_1 + 1.84F_2 - 9.78F_3 + 17.88F_4 + 1.98F_5 - 2.79F_3^2 - 2.41F_4^2 - 3.77X_1F_4 + 2.02X_3F_4 \quad (26)$$

The R-squared (R^2), the adjusted R-squared (Adj R^2) and the MS Residual (**Table 5**) statistically justified the correctness of the models. The values of R^2 (0.96056 and 0.97598 for OTC and Cd(II) respectively) and Adj R^2 (0.91753 and 0.94978 for OTC and Cd(II) respectively) are close to 1, confirming the goodness of the models and the high correlation between the predicted and the observed values.

Table 5.

The predicted versus observed values of OTC and Cd(II) removal efficiencies were plotted in **Fig. 4a, 4b**. These plots confirmed the model satisfactoriness and the appropriate agreement between the predicted and the experimental data.

Fig. 4.

Surface response studies

The correlation between factors and responses was graphically represented by 3D response surface plots. In this study, each figure (**Fig. 5a1-b3**) showed the effect of two tested factors on the OTC and Cd(II) adsorption, whereas all other factors were kept at fixed optimal levels. **Fig. 5a1** and **b1** show a 3D-view of the BBR response-surface efficiency to remove OTC and Cd(II) in function of time and pH. Firstly, it was observed that the removal of OTC and Cd(II) depended on the contact time. Indeed, the OTC and Cd(II) removal percentages increase with an increase in the reaction time during the first 20 h, until an equilibrium state was reached. As was explained by Harja et al. [53], during the initial stage of adsorption a large number of vacant sites on the BBR biosorbent surface were available for biosorption. With increasing reaction time, adsorption sites on the BBR surface become saturated. Furthermore, higher removal percentage of OTC was found at pH=6, at which this antibiotic had a zwitterionic form. In fact, the pKa values for OTC are 3.3 (amide group), 7.7 (hydroxyl and carbonyl

groups) and 9.9 (amine group) [54,55]. Consequently, OTC molecules can have a cationic, zwitterionic and anionic form, depending on the pH value of the solution [54,55]. Thus, higher removal percentage for OTC at pH=6 can be due to the attraction of OTC cationic groups ($R\text{-}N^{+}$) onto the negative surface of BBR, and/or π-π stacking interactions. In contrast, higher pH value increased Cd(II) adsorption. This can be explained by the existing electrostatic repulsion between cationic Cd(II) and positive BBR surface at low pH. At pH ranging from 4.7 to 8.1, the high Cd(II) biosorption efficiency can be explained by the electrostatic interaction between cationic Cd(II) and negative BBR surface. Moreover, at pH higher than 8.1, cadmium had a $Cd(OH)_2$ form [56]. In this case, Cd(II) adsorption cannot take place.

Fig. 5a2 and **b2** show the combined effect of contact time and adsorbent weight on OTC and Cd(II) biosorption efficiency. It seems that the increase of BBR mass resulted in an increase in OTC and Cd(II) removal percentages. This finding can be interpreted by the clear fact that more BBR surface provides more reactive biosorption sites, while lower amount of BBR adsorbent yielded significantly lower adsorption percentages, which emphasizes our previous explanation. Indeed, the decrease of active sites would result in lower ratio of contaminants molecule/ion to vacant sites and thus lesser removal efficiencies.

Finally, **Fig. 5a3** and **b3** show the binary effect of OTC and Cd(II) concentrations on the efficiency of the BBR to adsorb them. It was observed that the initial concentrations of antibiotic and heavy metal strongly affected BBR efficiency. In fact, it seems that the OTC and Cd(II) removal efficiencies decrease with increasing initial OTC and Cd(II) concentrations. This can be explained by the fact that high concentration of contaminant saturates the adsorbent surface area and prevents further adsorption capacity.

In addition, it can be clearly observed that the variation of OTC concentration did not affect Cd(II) removal. Whereas, OTC removal percentage slightly increases with increasing initial Cd(II) concentration. At pH = 6, Cd(II) species were present in the solution. The Cd(II) cationic species could combine with the negatively charged sites on the BBR surface, acting as a bridge between OTC and BBR particles. This cationic bridging has been reported by several researchers as one of the mechanisms for the adsorption of OTC [2,57]. In addition, the increase of OTC biosorption on the adsorbent surface in the presence of Cd(II) could be also related to the formation of OTC-Cd complexes. The predominant OTC species at a solution pH equal to 6 was OTC^{+-}, which could robustly combine with Cd(II) to form a Cd-OTC^{2+} complex. This OTC-Cd complex had less negative surface charge and was more easily

biosorbed on BBR surfaces than OTC itself under high pH conditions. This mechanism has been also reported for Tetracycline sorption on sediments [58] and soils [59].

Fig. 5.

Response optimization by desirability function (DF) for biosorption process

Fig. 6 illustrates the profiles for the predicted values, the optimization plots, and the desirability option for the OTC and Cd(II) adsorption from binary system. The desirability was defined as a function of a specified response that may be used for optimization of independent parameters [60]. As shown in **Fig. 6**, firstly, the maximum adsorption values (desirability of 1.0) under the optimum conditions were 63.66 % and 99.99 % for OTC and Cd(II), respectively. Secondly, the mean biosorption values (desirability of 0.5) were 35.57 % and 52.35 % of OTC and Cd(II), respectively. Finally, the minimum biosorption values (desirability of 0.0) of OTC was 7.48 % and that of Cd(II) was 4.70 %. For a desirability score of 1.0, the maximum responses of 63.66 % and 99.99 % OTC and Cd(II), respectively, were obtained under the following optimal conditions: 4.19 g L^{-1} adsorbent, 165.54 µmol L^{-1} OTC, 362.16 µmol L^{-1} Cd(II), pH 6 and 25.14 h contact time.

Fig. 6.

Non-linear-kinetic modeling of antibiotic and heavy metal adsorption

Fig. 7 shows the kinetic curves for OTC and Cd(II) adsorption. These curves show an initial state where a relatively rapid adsorption takes place up to an equilibrium state for OTC, and especially for Cd(II). Indeed, the states of equilibrium were reached at 20 h and at 5 h for OTC and Cd(II), respectively. In addition, at equilibrium, biosorption efficiency values were found to be 12.57 mg g^{-1} and 9.72 mg g^{-1} for OTC and Cd(II), respectively. **Table S3** illustrates the calculated data from the non-linear-fit of the six studied models. The R^2 values of all used kinetic models were higher than 0.88454 and 0.99950 for OTC and Cd(II), respectively, proving a good adequacy of the kinetic models for the adsorption of both pollutants. By comparing the values of R^2, the OTC adsorption mechanism appeared to be well described by the BSf equation. Moreover, the obtained experimental 12.57 mg g^{-1} value and the predicted 12.65 mg g^{-1} value of maximum biosorption capacity (q_m) for OTC adsorption were very close. Furthermore, by comparing the X^2 and RSS values, the most accurate description of the OTC adsorption mechanism was obtained by the BSf model. Regarding the BSf equation, in view of it being a general equation that includes all the other ones, fits were performed for various Brouers-Sotolongo models. On the basis of the R^2, the

(X^2), and the RSS values, the best non-linear fit for OTC adsorption was observed with the Weibull model. For the Cd(II) adsorption, the R^2 value of Weibull model was equal to 0.99950. Yet, the comparison of the X^2 and RSS values confirmed that the most accurate description of the Cd(II) adsorption mechanism was achieved by the Weibull model. Fits were carried out for three values of n (1, 1.5 and 2). The best non-linear fits for OTC and Cd(II) adsorption were observed with the n=1 order. These results showed the high heterogeneity of the studied system, involving sorbing materials with different chemical and structural characteristics [61]**.**

Fig. 7.

Table. S3 (Supplementary Material)

Equilibrium isotherms for antibiotic and heavy metal adsorption

The isotherm study of OTC and Cd(II) biosorption was performed at the optimal conditions, obtained by CCD analysis. **Fig. 8** shows the isotherm curves of OTC and Cd(II) biosorption on BBR, from binary system, according to the already mentioned models. **Table S4** contains all isotherm parameters obtained by non-linear fitting. Firstly, based on the R^2 values, the Freundlich, and Jovanovich models were more suitable for adjusting the biosorption isotherms of OTC. This result was also confirmed by the maximum adsorption capacity (15.78 mg g^{-1}), which is very close to the experimental value (16.05 mg g^{-1}), and the low X^2 and RSS values obtained using the Freundlich, and Jovanovich fits. Secondly, by comparing the values of R^2, the Cd(II) adsorption mechanism appeared to be well described by the GBS equation. Yet, the obtained experimental 23.54 mg g^{-1} value and the predicted 23.95 mg g^{-1} value of maximum biosorption capacity (q_m) for Cd(II) adsorption were very close. Moreover, by comparing the X^2 and RSS values, the most accurate description of the Cd(II) adsorption mechanism was obtained by the GBS model. In this case, due to the fact of the GBS model being a general equation that includes all the other isotherms, fits were performed for various Brouers-Sotolongo models. On the basis of the R^2, the X^2, and the RSS values, the BS model seemed more suitable for Cd(II) biosorption. The fits were made with various values of c (0, 0.5 and 1). Hence, the best fit, yielding the highest R^2 coefficient, was obtained with the Freundlich/Jovanovich and BS equations for the biosorption of OTC and Cd(II) respectively, where c=0. In line with previous findings by Karoui et al. [30], Brouers and AlMusawi [61], and Stanislavsky and Weron [62], this work considers the fact that c=0 is a sign of the existence of active sites, heterogeneous adsorption interactions, and great heterogeneity of the BBR surface. The isotherm study would imply firstly that the surface energy is heterogeneous

and the adsorbed molecular species interact among them to form a contaminants poly-layer. Secondly, these results confirm the high heterogeneous systems. Finally, the adsorption process of OTC and Cd(II) imply sorbing materials with various structural and chemical characteristics.

Fig. 8.

Table. S4 (Supplementary Material)

Biosorption thermodynamics

The spontaneity, endothermic or exothermic nature of the adsorption phenomenon of binary OTC and Cd(II) onto BBR were evaluated using the enthalpy (ΔH^0), entropy (ΔS^0), and Gibbs free energy (ΔG^0). The Equations (27)-(30) and the plotting ln(K_d) versus 1/T were used to determine the mentioned basic thermodynamic parameters [63–66]:

$$\Delta G^0 = \Delta H^0 - T\Delta S^0 \qquad (27)$$

$$K_d = \frac{q_e}{C_e} \qquad (29)$$

$$\ln K_d = \frac{\Delta S^0}{R} - \frac{\Delta H^0}{RT} \qquad (30)$$

where, T represents the absolute temperature (K); R is the universal gas constant (8.314 J.mol/K); and K_d is the distribution coefficient.

The linear plot of lnK_d against 1/T is given in **Fig. S4**.

Fig. S4. (Supplementary Material)

All thermodynamic data are illustrated in **Table 6**. The negative values of ΔG^0 obtained at different temperatures demonstrated the thermodynamic spontaneity of the adsorption reaction [30].

It seems that the increase of temperature resulted in a decrease in the ΔG^0 values and an increase in the Kd values. This result implied that OTC and Cd(II) adsorption is more favorable at high temperature, through the improvement of the adsorption capacity of BBR surface. The ΔH^0 values were 22.76 kJ mol^{-1} and 35.72 kJ mol^{-1}, for OTC and Cd(II) adsorption, respectively. The mentioned positive values of ΔH^0 indicated that OTC and Cd(II)

adsorption was endothermic. Furthermore, the ΔH^0 values were lesser than 80 kJ/mol, indicating the physical nature of OTC and Cd(II) adsorption onto BBR. The ΔS^0 values were 70.28 J/mol.k and 204.94 J/mol.k, for OTC and Cd(II) biosorption, respectively. These positive values suggest the increased randomness at the solid/solution interface during the adsorption of OTC and Cd(II) by BBR. Similar results were found in many thermodynamic studies about adsorption of antibiotic and heavy metal onto various biomaterials [67,68]. Finally, by comparing thermodynamic parameters of OTC and Cd(II), it seemed that the adsorption of Cd(II) is faster than the OTC adsorption, due to the affinity and the stronger interaction between the BBR surface and Cd(II) cations. This result confirms the isotherm studies.

Table 6.

Suggested biosorption mechanism

BBR is a reed-based composite. The reed is mainly composed of celluloses, hemicelluloses and lignin. The FTIR, MEB analysis and modeling study confirmed the chemical and physical heterogeneity of the BBR surface. BBR biocomposite was then rich in carbonyls, hydroxyls, ethers, aldehydes, phenols, aldehydes, and aromatic compounds. The optimum pH for OTC and Cd(II) biosorption was found to be 6, using CCD analysis. At this pH, the BBR surface (pH_{pzc} = 4.7) was negatively charged. Consequently, the adsorption of Cd(II) cations takes place through electrostatic attraction between them and the BBR surface. Knowing that OTC pKa_1, pKa_2 and pKa_3 values were 3.3, 7.7 and 9.9 respectively, at pH 6, OTC would have a zwitterionic form (OTC^{+-}) and electrostatic interaction between the OTC cationic groups ($R\text{-}N^+$) and the BBR surface would occur. The biosorption of OTC could also take place via π-π stacking, as well as hydrophobic interactions, as shown in **Fig. 9**.

According to the CCD application and FTIR analysis, the formation of BBR-O≡Cd-OTC ternary complex could take place. This complex would be caused by an electrostatic interaction between the cationic Cd(II) and the anionic group (COO^-) of OTC. Moreover, the explanation of OTC and Cd(II) adsorption through the BBR pores would be equally possible.

Fig. 9.

Regeneration study

The regeneration study of binary OTC and Cd(II) biosorption was performed at the optimal conditions, obtained by CCD analysis. Desorption experiments were used to regenerate the biosorbent and recover the antibiotic and heavy metal. In this study, ultra-pure water, 0.1 M HCl, and 0.1 M CH_3COOH were examined as eluents. The obtained results are illustrated in **Fig. 10 a1 and a2.** The maximum percentage recovery of OTC was 92.44% with 0.1M CH_3COOH, whereas that of Cd(II) was 99.96% with ultra-pure water in the first cycle. It was found that 0.1M CH_3COOH and ultra-pure water were good eluents for desorption of OTC and Cd(II), respectively, compared to other assessed eluents.

The strong desorption efficiency of CH_3COOH may simply be explained by the electrostatic repulsion occurring between the BBR adsorbent and OTC antibiotic, due to the fact that both acquired positive charges in an acidic medium.

Then, 1M CH_3COOH and ultra-pure water were used as an eluent agent for OTC and Cd(II), respectively. The regenerated biosorbent was reused for three adsorption-desorption cycles, as shown in **Fig. 10. b1** and **b2**. A gradual decrease in OTC and Cd(II) adsorption efficiency with the increase in the cycle's number was observed. After a sequence of three cycles, the adsorption capacities of the BBR adsorbent were reduced from 63.65 % to 56.78 % for OTC, and from 99.99 % to 98.68 % for Cd(II). The loss in the biosorption capacity of the biosorbent for antibiotic and heavy metal ions were 6.87 % for OTC and 1.31 % for Cd(II). This might be due to the alteration of the BBR adsorbent and/or the ignorable weight loss of BBR biosorbent during the adsorption-desorption process. Therefore, BBR could be used for three cycles in OTC and Cd(II) biosorption with a small loss in its biosorption capacity.

Conclusion

In this study, a reed-based-beads biocomposite was developed from an invasive reed plant, to be used as adsorbent, which would be easy to produce, efficient and cost effective. A detailed characterization of the BBR beads showed that this biocomposite was made of celluloses, hemicelluloses and lignin, which indicate its potential as enhanced adsorbent. The BBR beads were also characterized after OTC and Cd(II) adsorption, finding that the biosorption process was successfully implemented. Moreover, the optimization of the biosorption was achieved through the combination of five factors; namely, the adsorbent amount, the OTC concentration, the Cd(II) concentration, the pH, and the reaction time. The optimal conditions were found to be 4.19 g L^{-1} of biosorbent, 165.54 µmol L^{-1} of OTC, 362.16 µmol L^{-1} of Cd(II), a pH of 6, and 25.14 h contact time. This study proved that at the mentioned optimal

conditions, the percentages of adsorption would reach 63.66 % and 99.99 % for OTC and Cd(II), respectively. Furthermore, at equilibrium, biosorption efficiency values were 16.05 mg g^{-1} and 23.54 mg g^{-1} for OTC and Cd(II), respectively. Therefore, the current study showed that the developed biosorbent is economic and effective for the simultaneous uptake of OTC and Cd(II) from aqueous solution. Regarding the elucidation of mechanisms involved in the simultaneous biosorption of OTC and Cd(II) onto BBR, the kinetic study showed that the adsorption of Cd(II) was faster than that of OTC. Indeed, the states of equilibrium were reached at 20 h and at 5 h for OTC and Cd(II), respectively. OTC and Cd(II) adsorption mechanisms were described by the BSf equation and the Weibull model, respectively. The isotherm study confirmed that the biosorbent surface was heterogeneous and the Freundlich/Jovanovich and BS equations led to the best non-linear fits for the biosorption of OTC and Cd(II), respectively. Furthermore, the BBR efficiency was assessed thermodynamically, showing that higher temperature favored better biosorption percentages, reaching up to 80.58 % and 100 % for OTC and Cd(II), respectively, at 50 °C. Furthermore, it was shown that the biosorption mechanisms for OTC and Cd(II) are physisorption, spontaneous and endothermic. The adsorption mechanisms took place through the electrostatic interactions between the Cd(II) cations and the anionic groups (COO-, OH) of the BBR adsorbent, and/or via π-π stacking interactions between lignin aromatic groups of BBR and OTC pollutant. In addition, electrostatic interaction between the OTC cationic groups ($R\text{-}N^{+}$) and the BBR surface, would occur. The formation of BBR-O≡Cd-OTC ternary complex could take place. This complex would be caused by electrostatic interactions between the cationic Cd(II) and the anionic (C=O) groups of OTC. Moreover, the explanation of OTC and Cd(II) adsorption through the BBR pores and through formation of BBR-O≡Cd-OTC ternary complex would be also possible. Overall, the main objective of this work being to promote the valorizing of the reed plant and ridding the aquatic environment of large amounts of polluted wastewater at little expenses, was successfully reached, which would be of aid to facilitate an improvement of environmental health.

References

[1] A. Hartmann, E.M. Golet, S. Gartiser, A.C. Alder, T. Koller, R.M. Widmer, Primary DNA damage but not mutagenicity correlates with ciprofloxacin concentrations in German hospital wastewaters, 119 (1999) 115–119.

[2] J.R. V Pils, D.A. Laird, Sorption of tetracycline and chlortetracycline on K- and Ca-saturated soil clays, humic substances, and clay-humic complexes, Environmental Science and Technology. 41 (2007) 1928–1933. doi:10.1021/es062316y.

[3] F. Lian, Z. Song, Z. Liu, L. Zhu, B. Xing, Mechanistic understanding of tetracycline sorption on waste tire powder and its chars as affected by Cu 2 þ and pH, Environmental Pollution. 178 (2013) 264–270. doi:10.1016/j.envpol.2013.03.014.

[4] X. Xu, X. Li, Chemosphere Sorption and desorption of antibiotic tetracycline on marine sediments, Chemosphere. 78 (2010) 430–436. doi:10.1016/j.chemosphere.2009.10.045.

[5] N. Suga, M. Ogo, S. Suzuki, Risk assessment of oxytetracycline in water phase to major sediment bacterial community : A water-sediment microcosm study, Environmental Toxicology and Pharmacology. 36 (2013) 142–148. doi:10.1016/j.etap.2013.03.013.

[6] H. Mihciokur, M. Oguz, Removal of oxytetracycline and determining its biosorption properties on aerobic granular sludge, Environmental Toxicology and Pharmacology. 46 (2016) 174–182. doi:10.1016/j.etap.2016.07.017.

[7] F. Fu, Q. Wang, Removal of heavy metal ions from wastewaters : A review, Journal of Environmental Management. 92 (2011) 407–418. doi:10.1016/j.jenvman.2010.11.011.

[8] A. Aghababaei, M.C. Ncibi, M. Sillanpää, Optimized removal of Oxytetracycline and Cadmium from contaminated waters using chemically-activated and pyrolyzed biochars from forest and wood-processing residues, Bioresource Technology. (2017). doi:10.1016/j.biortech.2017.04.119.

[9] S. Li, X. Li, D. Wang, Membrane (RO-UF) filtration for antibiotic wastewater treatment and recovery of antibiotics, 34 (2004) 109–114. doi:10.1016/S1383-5866(03)00184-9.

[10] M. Soylak, U. Divrikli, S. Saracoglu, Membrane filtration – atomic absorption spectrometry combination for copper , cobalt , cadmium , lead and chromium in environmental samples, (2007) 169–176. doi:10.1007/s10661-006-9271-0.

[11] W. Li, Q. Wang, Removal of Tetracycline and Oxytetracycline in Water by a Reverse Osmosis Membrane, 2009 3rd International Conference on Bioinformatics and Biomedical Engineering. (2009) 1–4. doi:10.1109/ICBBE.2009.5163315.

[12] P. Taylor, S. Bayar, A.E. Yilmaz, R. Boncukcuo, B.A. Fìl, M. Muhtar, B.A. Fil, S. Bayar, A.E. Yilmaz, R. Boncukcuog, Desalination and Water Treatment Effects of operational parameters on cadmium removal from aqueous solutions by electrochemical coagulation aqueous solutions by electrochemical coagulation, (n.d.) 37–41. doi:10.1080/19443994.2012.749201.

[13] J. Issn, F.A. Online, Coagulation / flocculation process in the removal of trace metals present in industrial wastewater, (2006) 1–4.

[14] Q. Chen, S. Wu, Y. Xin, Synthesis of Au – CuS – TiO 2 nanobelts photocatalyst for efficient photocatalytic degradation of antibiotic oxytetracycline, 302 (2016) 377–387. doi:10.1016/j.cej.2016.05.076.

[15] T. Watanabe, T. Taklzawa, K. Honda, Photocatalysis through Excitation ot Adsorbates . 1 . Highly Efficient / V-Deethylation of Rhodamine B Adsorbed to CdS, 81 (1977) 1845–1851. doi:10.1021/j100534a012.

[16] I.L.A.K.B. Alciog, Simultaneous Removal of Oxytetracycline and Sulfamethazine Antibacterials from Animal Waste by Chemical Oxidation Processes, (2009) 11284–11291. doi:10.1021/jf902188j.

[17] A. Alwash, Study on the Catalytic Activity of Cerium / Cadmuim Mixed Oxide Catalysts for the Photo catalytic Degradation of Orange G Dye Keywords :, 20 (2017) 71–79.

[18] E. Maliou, M. Malamis, P.O. Sakellarides, LEAD AND CADMIUM REMOVAL BY ION EXCHANGE, 25 (2018) 133–138.

[19] W. Sun, Y. Sun, K.J. Shah, H. Zheng, B. Ma, Electrochemical degradation of oxytetracycline by Ti-Sn-Sb / γ-Al 2 O 3 three- dimensional electrodes, Journal of

Environmental Management. 241 (2019) 22–31. doi:10.1016/j.jenvman.2019.03.128.

[20] S. Farhadi, F. Siadatnasab, Sonocatalytic degradation of organic pollutants by CdS nanoparticles hydrothermally prepared from cadmium (II) diethanoldithiocarbamate, 66 (2017) 5004. doi:10.5004/dwt.2016.0096.

[21] J. Qiao, H. Zhang, G. Li, S. Li, Z. Qu, M. Zhang, J. Wang, Fabrication of a novel Z-scheme SrTiO 3 / Ag 2 S / CoWO 4 composite and its application in sonocatalytic degradation of tetracyclines, 211 (2019) 843–856. doi:10.1016/j.seppur.2018.10.058.

[22] Adsorption of cadmium(II) from aqueous solution onto activated carbon, Water Science and Technology. 35 (1997) 205–211. doi:10.1016/S0273-1223(97)00132-7.

[23] I. Sciences, S. Reclamation, E. Science, Adsorption and Desorption of Oxytetracycline and Carbamazepine by Multiwalled Carbon Nanotubes, (2009) 9167–9173. doi:10.1021/es901928q.

[24] M. Gaouar-Yadi, K. Tizaoui, N. Gaouar-Benyelles, B. Benguella, Efficient and eco-friendly adsorption using low-cost natural sorbents in waste water treatment, Indian Journal of Chemical Technology. 23 (2016) 204–209.

[25] R. Ben Arfi, S. Karoui, K. Mougin, A. Ghorbal, Adsorptive removal of cationic and anionic dyes from aqueous solution by utilizing almond shell as bioadsorbent, Euro-Mediterranean Journal for Environmental Integration. 2 (2017) 20. doi:10.1007/s41207-017-0032-y.

[26] Q. Song, Y. Fang, C. Cao, J. Liang, Z. Liu, L. Li, Y. Huang, J. Lin, C. Tang, Selective Adsorption Behavior/Mechanism of Antibiotic Contaminants on Novel Boron Nitride Bundles, Journal of Hazardous Materials. (2018). doi:10.1016/j.jhazmat.2018.10.054.

[27] Y. Zhang, Y. Wang, H. Zhang, Y. Li, Z. Zhang, W. Zhang, Resources , Conservation & Recycling Recycling spent lithium-ion battery as adsorbents to remove aqueous heavy metals : Adsorption kinetics , isotherms , and regeneration assessment, Resources, Conservation & Recycling. 156 (2020) 104688. doi:10.1016/j.resconrec.2020.104688.

[28] S. Altenor, B. Carene, E. Emmanuel, J. Lambert, J.J. Ehrhardt, S. Gaspard, Adsorption studies of methylene blue and phenol onto vetiver roots activated carbon prepared by

chemical activation, Journal of Hazardous Materials. 165 (2009) 1029–1039. doi:10.1016/j.jhazmat.2008.10.133.

[29] Y. Wan, Y. Bao, Q. Zhou, Chemosphere Simultaneous adsorption and desorption of cadmium and tetracycline on cinnamon soil, Chemosphere. 80 (2010) 807–812. doi:10.1016/j.chemosphere.2010.04.066.

[30] S. Karoui, R. Ben Arfi, K. Mougin, A. Ghorbal, A.A. Assadi, A. Amrane, Synthesis of novel biocomposite powder for simultaneous removal of hazardous ciprofloxacin and methylene blue : Central composite design , kinetic and isotherm studies using Brouer-Sotolongo family models, Journal of Hazardous Materials. (2019) 121675.

[31] R. Ben Arfi, S. Karoui, K. Mougin, A. Ghorbal, Cetyltrimethylammonium bromide-treated Phragmites australis powder as novel polymeric adsorbent for hazardous Eriochrome Black T removal from aqueous solutions, Polymer Bulletin. 76 (2018) 5077–5102.

[32] Z. Parsaee, N. Karachi, S.M. Abrishamifar, M.R.R. Kahkha, R. Razavi, Silver-choline chloride modified graphene oxide: Novel nano-bioelectrochemical sensor for celecoxib detection and CCD-RSM model, Ultrasonics Sonochemistry. 45 (2018) 106–115. doi:10.1016/j.ultsonch.2018.03.009.

[33] A.M. Ben Hamissa, F. Brouers, M.C. Ncibi, M. Seffen, Kinetic Modeling Study on Methylene Blue Sorption onto Agave americana fibers: Fractal Kinetics and Regeneration Studies, Separation Science and Technology (Philadelphia). 48 (2013) 2834–2842. doi:10.1080/01496395.2013.809104.

[34] S. Gaspard, S. Altenor, N. Passe-Coutrin, A. Ouensanga, F. Brouers, Parameters from a new kinetic equation to evaluate activated carbons efficiency for water treatment, Water Research. 40 (2006) 3467–3477. doi:10.1016/j.watres.2006.07.018.

[35] M. Saad, H. Tahir, J. Khan, U. Hameed, A. Saud, Synthesis of polyaniline nanoparticles and their application for the removal of Crystal Violet dye by ultrasonicated adsorption process based on Response Surface Methodology, Ultrasonics Sonochemistry. 34 (2017) 600–608.

[36] B. Sadhukhan, N.K. Mondal, S. Chattoraj, Optimisation using central composite design (CCD) and the desirability function for sorption of methylene blue from aqueous

solution onto Lemna major, Karbala International Journal of Modern Science. 2 (2016) 145–155. doi:10.1016/j.kijoms.2016.03.005.

[37] F. Brouers, O. Sotolongo-Costa, Generalized fractal kinetics in complex systems (application to biophysics and biotechnology), Physica A: Statistical Mechanics and Its Applications. 368 (2006) 165–175. doi:10.1016/j.physa.2005.12.062.

[38] F. Brouers, T.J. Al-Musawi, Brouers-Sotolongo fractal kinetics versus fractional derivative kinetics: A new strategy to analyze the pollutants sorption kinetics in porous materials, Journal of Hazardous Materials. 350 (2018) 162–168. doi:10.1016/j.jhazmat.2018.02.015.

[39] S. Larous, A.H. Meniai, Adsorption of Diclofenac from aqueous solution using activated carbon prepared from olive stones, International Journal of Hydrogen Energy. 41 (2016) 10380–10390. doi:10.1016/j.ijhydene.2016.01.096.

[40] L.R. Bonetto, F. Ferrarini, C. De Marco, J.S. Crespo, R. Guégan, M. Giovanela, Removal of methyl violet 2B dye from aqueous solution using a magnetic composite as an adsorbent, Journal of Water Process Engineering. 6 (2015) 11–20. doi:10.1016/j.jwpe.2015.02.006.

[41] Z.L. Yaneva, N. V Georgieva, Insights into Congo Red Adsorption on Agro-Industrial Materials - Spectral , Equilibrium , Kinetic , Thermodynamic , Dynamic and Desorption Studies . A Review, 4 (2012) 127–146.

[42] T.A.S. Ali Ahmed Alshaheri, Mohamed Ibrahim Mohamed Tahir, Mohd Basyaruddin Abdul Rahman, Thahira Begum, Synthesis, characterisation and catalytic activity of dithiocarbazate Schiff base complexes in oxidation of cyclohexane, Journal of Molecular Liquids. 240 (2017) 486--496. doi:10.1016/j.molliq.2017.05.081.

[43] H. Guedidi, B. Slama, Préparation et modification de carbones activés pour l ’ adsorption de polluants organiques émergents : molécules pharmaceutiques et liquides ioniques, 2016.

[44] X. Song, D. Liu, G. Zhang, M. Frigon, X. Meng, K. Li, Bioresource Technology Adsorption mechanisms and the effect of oxytetracycline on activated sludge, Bioresource Technology. 151 (2014) 428–431. doi:10.1016/j.biortech.2013.10.055.

[45] W.H. Danial, Z.A. Majid, M. Nazlan, M. Muhid, S. Triwahyono, M.B. Bakar, Z. Ramli, The reuse of wastepaper for the extraction of cellulose nanocrystals, Carbohydrate Polymers. 118 (2014) 165–169.

[46] P. Taylor, D.R. Manenti, D.E.G. Trigueros, A.P. De Oliveira, C.E. Borba, A.D. Kroumov, pt us, (2015) 37–41. doi:10.1080/09593330.2015.1051591.

[47] T. Oxidation, L. Jiao, H. Bian, Y. Gao, X. Lin, W. Zhu, H. Dai, Highly Dispersible Cellulose Nanofibrils Produced via Mechanical Pretreatment Highly Dispersible Cellulose Nanofibrils Produced via Mechanical Pretreatment and TEMPO-mediated Oxidation, (2018). doi:10.1007/s12221-018-8565-5.

[48] A. Alonso-simón, P. García-angulo, H. Mélida, A. Encina, J.M. Álvarez, J.L. Acebes, The use of FTIR spectroscopy to monitor modifications in plant cell wall architecture caused by cellulose biosynthesis inhibitors, (2011). doi:10.4161/psb.6.8.15793.

[49] C.S. Transactions, M.K. Mishra, Fourier Transform Infrared Spectrophotometry Studies of Chromium Trioxide-Phthalic Acid Complexes, 5 (2016) 770–774. doi:10.7598/cst2016.1260.

[50] R. Ben Arfi, S. Karoui, K. Mougin, A. Ghorbal, Adsorptive removal of cationic and anionic dyes from aqueous solution by utilizing almond shell as bioadsorbent, Euro-Mediterranean Journal For Environmental Integration. 2 (2017) 20.

[51] S.F. Montanher, E.A. Oliveira, M.C. Rollemberg, Removal of metal ions from aqueous solutions by sorption onto rice bran, 117 (2005) 207–211. doi:10.1016/j.jhazmat.2004.09.015.

[52] S. Mohan, G. Sreelakshmi, Fixed bed column study for heavy metal removal using phosphate treated rice husk, 153 (2008) 75–82. doi:10.1016/j.jhazmat.2007.08.021.

[53] M. Harja, G. Ciobanu, Studies on adsorption of oxytetracycline from aqueous solutions onto hydroxyapatite, Science of the Total Environment. 628–629 (2018) 36–43. doi:10.1016/j.scitotenv.2018.02.027.

[54] L. Aristilde, B. Lanson, L. Charlet, Interstratification patterns from the pH-dependent intercalation of a tetracycline antibiotic within montmorillonite layers, Langmuir. 29 (2013) 4492–4501. doi:10.1021/la400598x.

[55] S. Liu, P. Wu, L. Yu, L. Li, B. Gong, N. Zhu, Z. Dang, C. Yang, Preparation and characterization of organo-vermiculite based on phosphatidylcholine and adsorption of two typical antibiotics, Applied Clay Science. 137 (2017) 160–167. doi:10.1016/j.clay.2016.12.002.

[56] K.J. Powell, P.L. Brown, R.H. Byrne, T. Gajda, G. Hefter, S. Sjöberg, H. Wanner, Chemical speciation of environmentally significant metals with inorganic ligands Part 2: The Cu2+-OH-, Cl-, CO32-, SO42-, and PO43- systems (IUPAC Technical Report), Pure and Applied Chemistry. 79 (2007) 895–950. doi:10.1351/pac200779050895.

[57] S. Agriculture, Adsorption and Cosorption of Tetracycline and Copper (II) on Montmorillonite as Affected by Solution pH, 42 (2008) 3254–3259.

[58] G. Zhang, X. Liu, K. Sun, Y. Zhao, C. Lin, Sorption of tetracycline to sediments and soils : assessing the roles of pH , the presence of cadmium and properties of sediments and soils, 4 (2010) 421–429. doi:10.1007/s11783-010-0265-3.

[59] D. Jia, D. Zhou, Y. Wang, H. Zhu, J. Chen, Geoderma Adsorption and cosorption of Cu (II) and tetracycline on two soils with different characteristics, 146 (2008) 224–230. doi:10.1016/j.geoderma.2008.05.023.

[60] A. Asfaram, H. Sadeghi, A. Goudarzi, E.P. Kokhdan, Z. Salehpour, Ultrasound-assisted combined with manganese-oxide nanoparticles loaded DOI: 10.1039/C8AN02338G on activated carbon for extraction and pre-concentration of thymol and carvacrol in methanolic extracts of Thymus daenensis, Salvia officinalis, Stachys pilifer, (2019). doi:10.1039/C8AN02338G.

[61] F. Brouers, T.J. Al-Musawi, On the optimal use of isotherm models for the characterization of biosorption of lead onto algae, Journal of Molecular Liquids. 212 (2015) 46–51. doi:10.1016/j.molliq.2015.08.054.

[62] A. Stanislavsky, K. Weronb, Is there a motivation for a universal behaviour in molecular populations undergoing chemical reactions, Phys. Chem. Chem. Phys. 15 (2013) 15595–15601.

[63] N. Barka, K. Ouzaouit, M. Abdennouri, M. El Makhfouk, Dried prickly pear cactus (Opuntia ficus indica) cladodes as a low-cost and eco-friendly biosorbent for dyes removal from aqueous solutions, Journal of the Taiwan Institute of Chemical

Engineers. 44 (2013) 52–60. doi:10.1016/j.jtice.2012.09.007.

[64] R. Dutta, T. V. Nagarjuna, S.A. Mandavgane, J.D. Ekhe, Ultrafast removal of cationic dye using agrowaste-derived mesoporous adsorbent, Industrial and Engineering Chemistry Research. 53 (2014) 18558–18567. doi:10.1021/ie5030003.

[65] A. Mittal, V.K. Gupta, A. Malviya, J. Mittal, Process development for the batch and bulk removal and recovery of a hazardous, water-soluble azo dye (Metanil Yellow) by adsorption over waste materials (Bottom Ash and De-Oiled Soya), Journal of Hazardous Materials. 151 (2008) 821–832. doi:10.1016/j.jhazmat.2007.06.059.

[66] M. Ahmaruzzaman, Adsorption of phenolic compounds on low-cost adsorbents: A review, Advances in Colloid and Interface Science. 143 (2008) 48–67. doi:10.1016/j.cis.2008.07.002.

[67] F. Belaib, M. Azzedine, B. Boubeker, M. Abdeslam-hassen, Experimental study of oxytetracycline retention by adsorption onto polyaniline coated peanut shells, International Journal of Hydrogen Energy. 39 (2013) 1511–1515. doi:10.1016/j.ijhydene.2013.05.015.

[68] C. Hu, P. Zhu, M. Cai, H. Hu, Q. Fu, Comparative adsorption of Pb(II), Cu(II) and Cd(II) on chitosan saturated montmorillonite: Kinetic, thermodynamic and equilibrium studies, Applied Clay Science. 143 (2017) 320–326. doi:10.1016/j.clay.2017.04.005.

[69] K.V. Kumar, K. Porkodi, F. Rocha, Comparison of various error functions in predicting the optimum isotherm by linear and non-linear regression analysis for the sorption of basic red 9 by activated carbon, Journal of Hazardous Materials. 150 (2008) 158–165. doi:10.1016/j.jhazmat.2007.09.020.

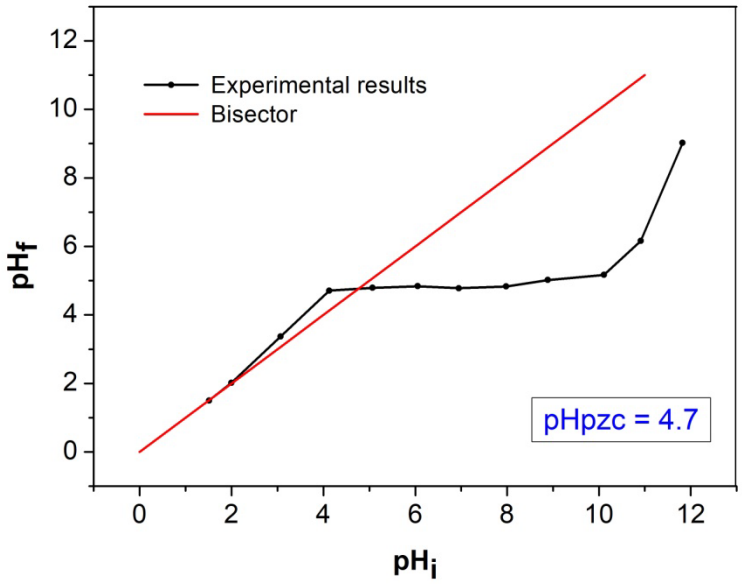

Fig. 1. pH_{PZC} of the BBR biocomposite beads (T = 20 ± 1 °C).

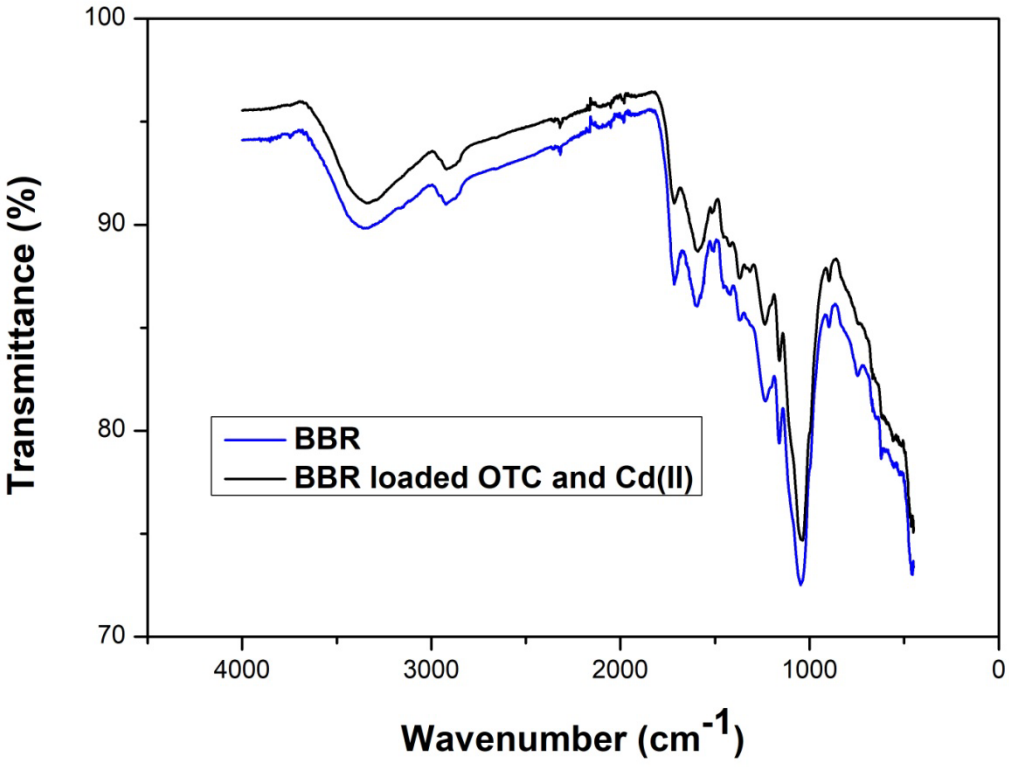

Fig. 2. FTIR-ATR spectra of the BBR (blue line), and BBR-OTC-Cd(II) (black line).

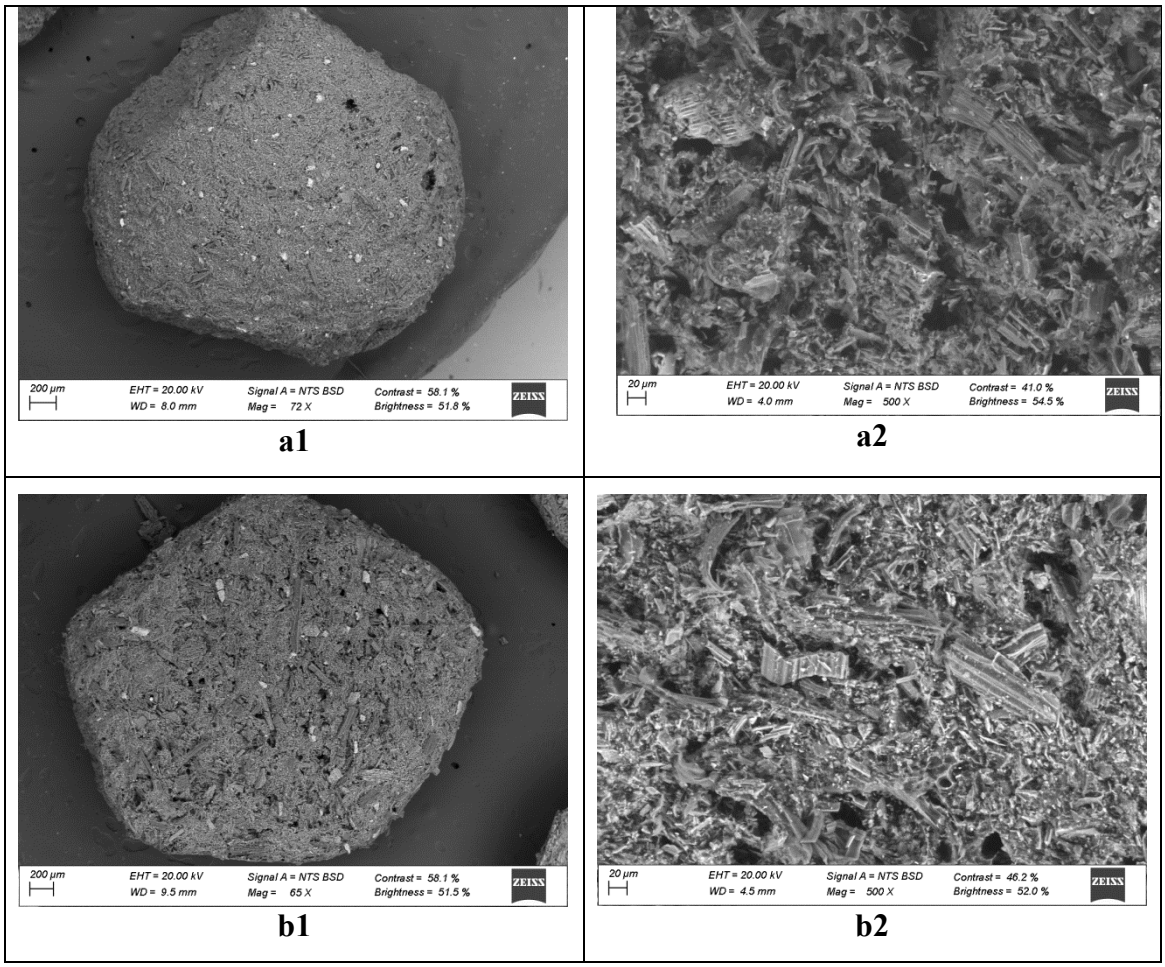

Fig. 3. SEM images of the BBR surface: **3a** SEM images of the BBR before adsorption **3b** SEM images of the BBR after OTC and Cd(II) adsorption.

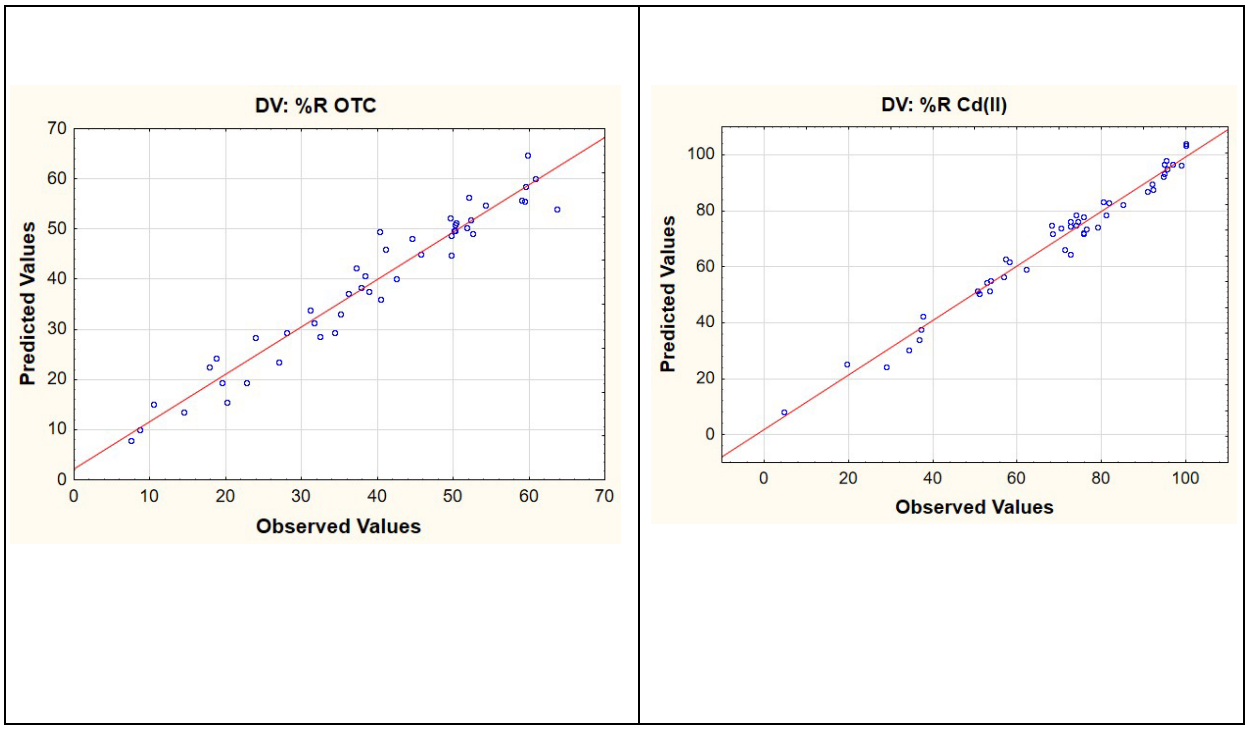

Fig. 4. Observed versus predicted responses (%R) for OTC and Cd(II) removal.

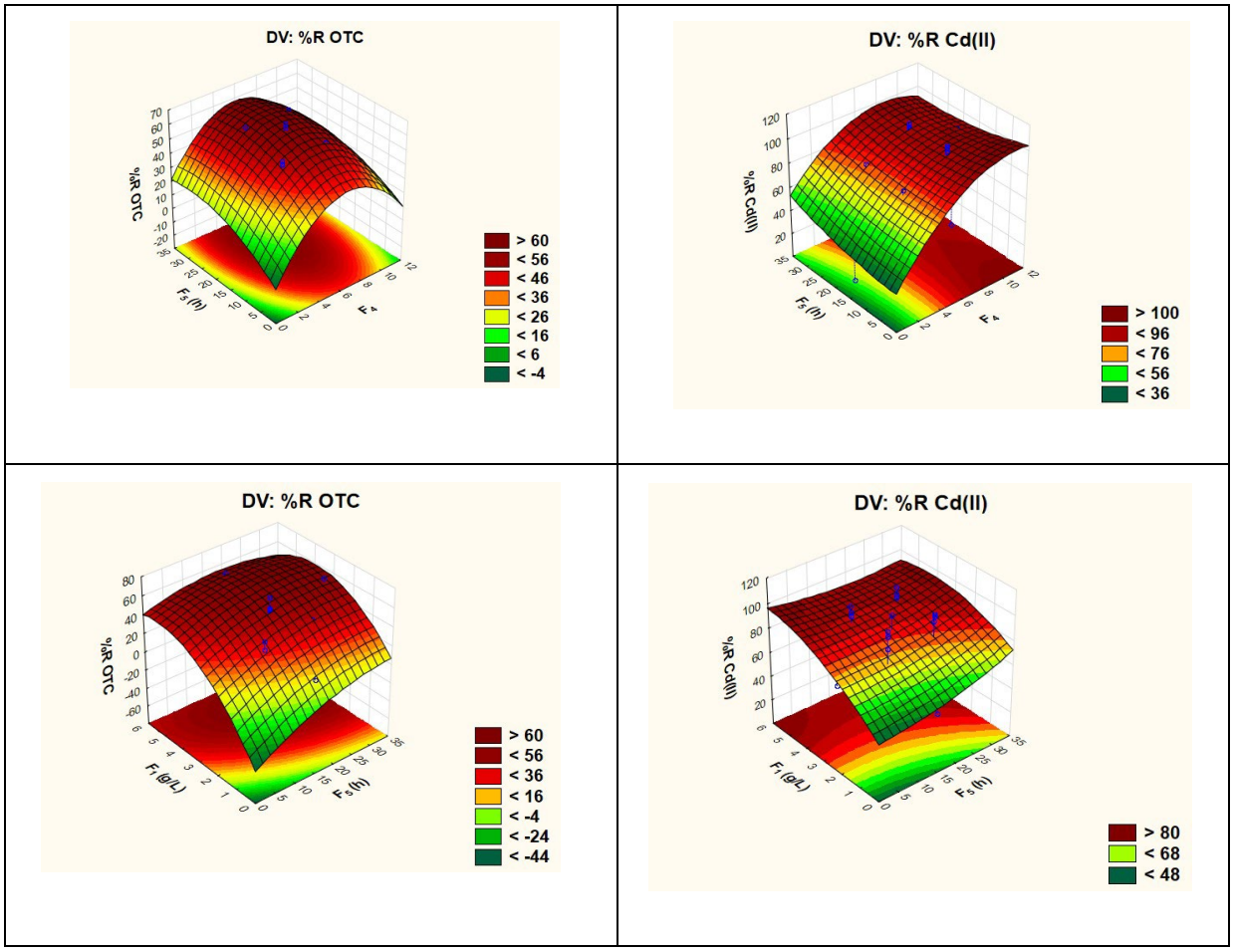

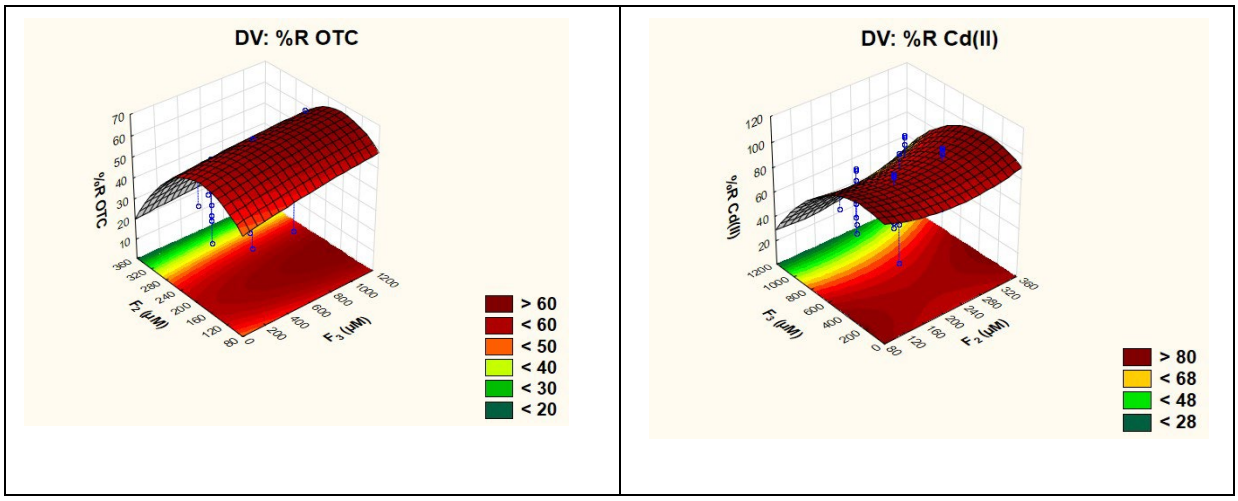

Fig. 5. Response surface plots for combined effect of **(a1, b1)** pH and reaction time; **(a2, b2)** adsorbent mass and reaction time; **(a3, b3)** OTC and Cd(II) concentrations, on biosorption efficiency of OTC and Cd(II).

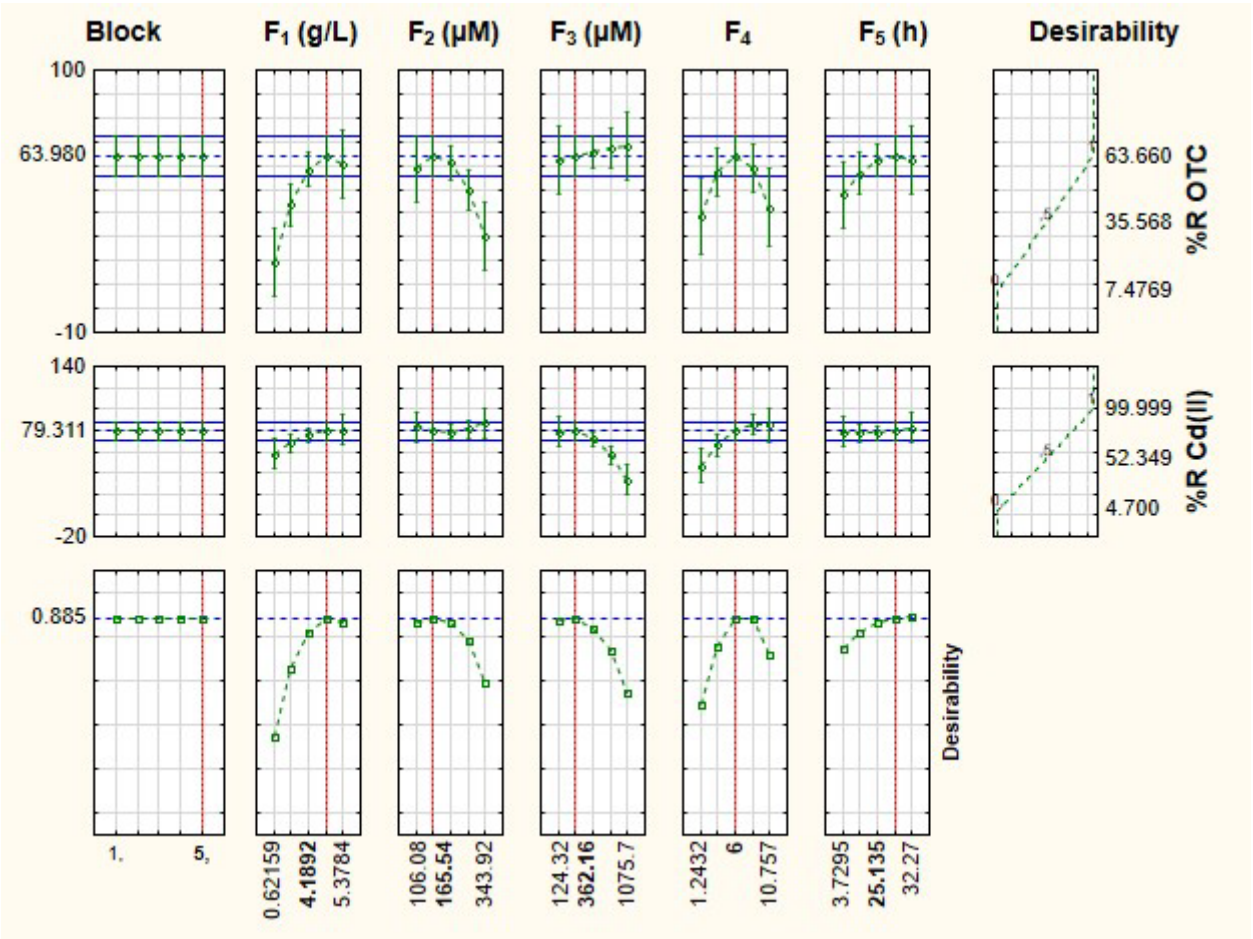

Fig. 6. Desirability function profile for simultaneous biosorption of of OTC and Cd(II). Dashed red line indicated optimized values.

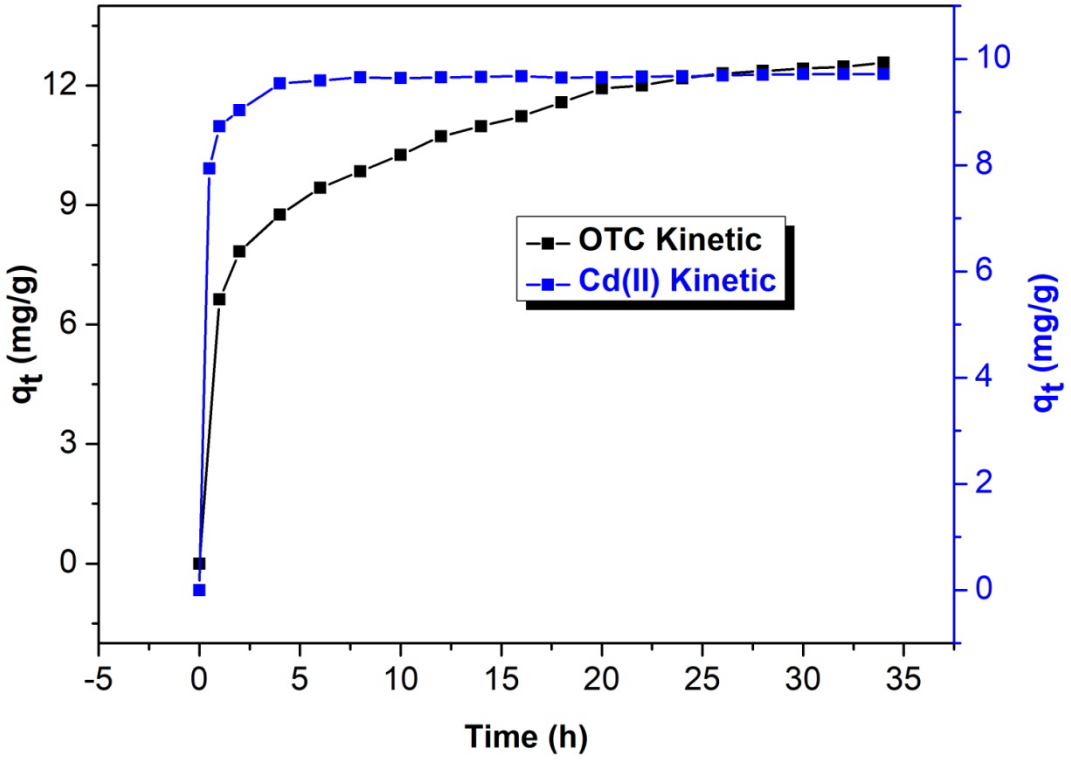

Fig. 7. kinetic curves for the OTC and Cd(II) adsorption from binary system (F_1 = 4.1892 g/L ; F_2 = 165.54 µM ; F_3 = 362.16 µM ; X_4 = 6 ; X_5 = 25.135 h ; T = 20 ± 1 °C).

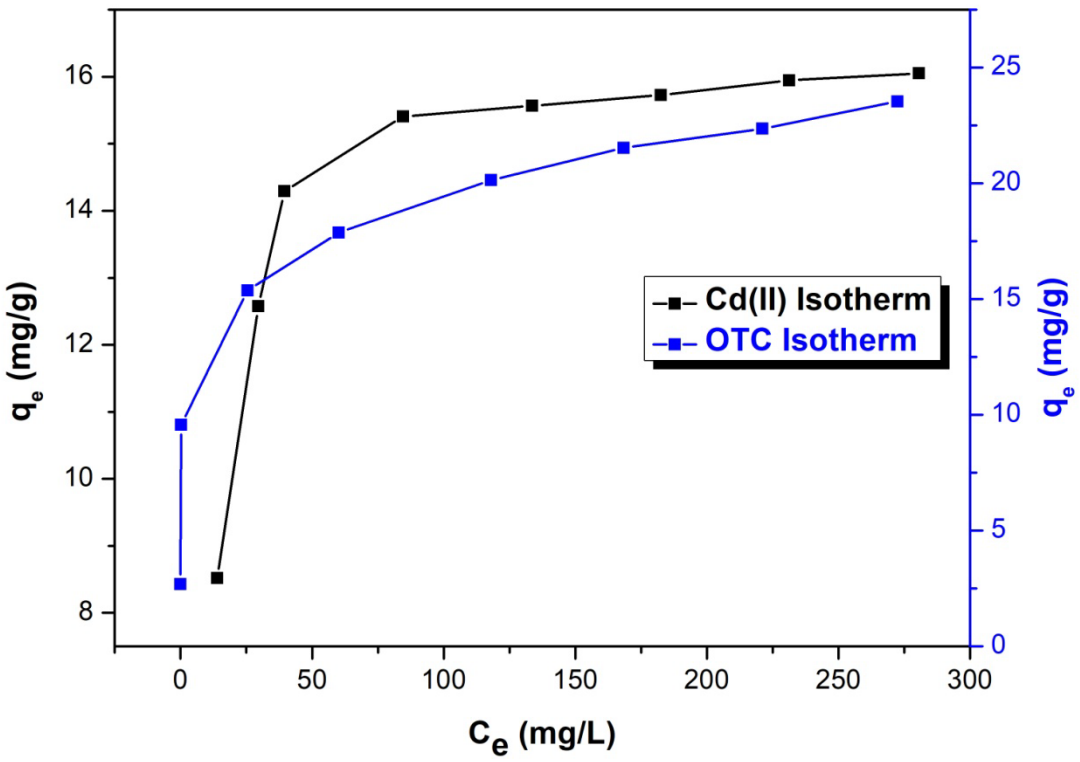

Fig. 8. isotherm curves for the OTC and Cd(II) adsorption from binary system (F_1 = 4.1892 g/L ; F_2 = 165.54 µM ; F_3 = 362.16 µM ; X_4 = 6 ; X_5 = 25.135 h ; T = 20 ± 1 °C).

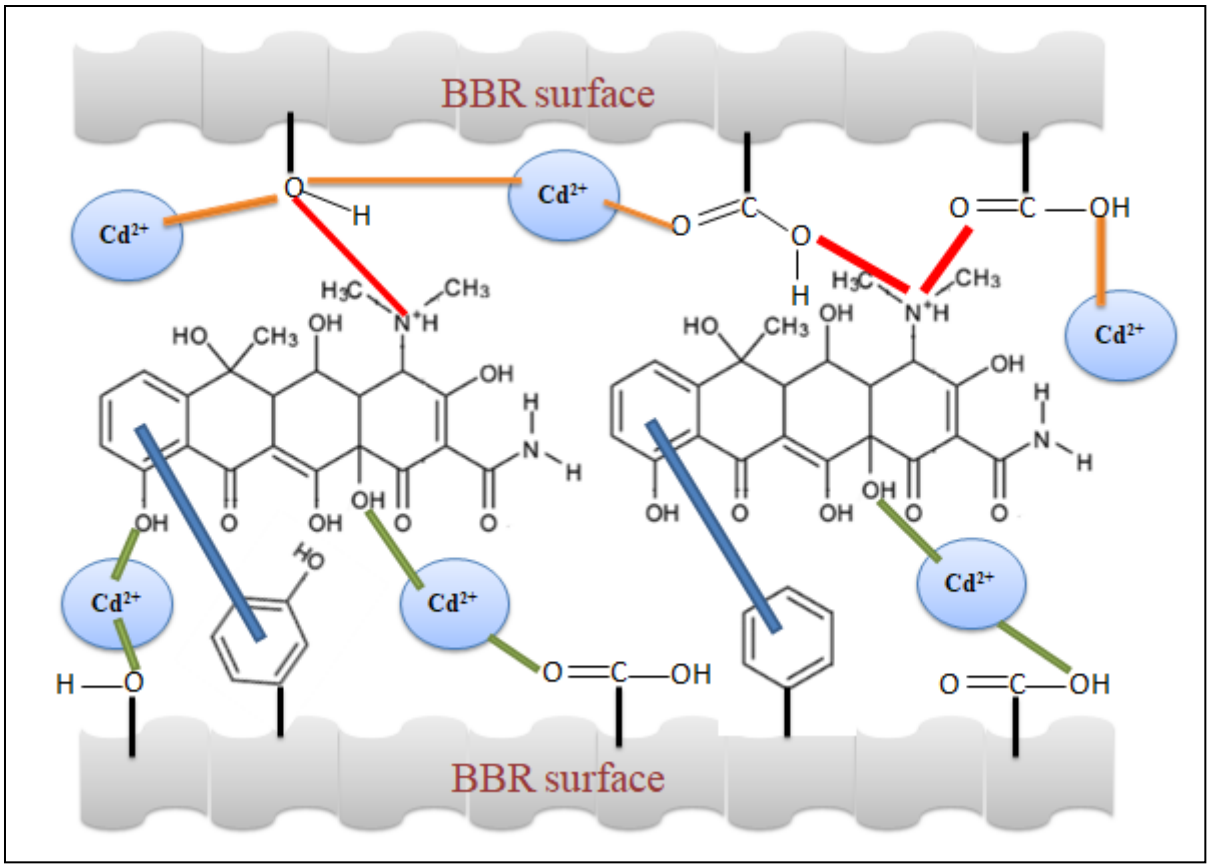

Fig. 9. Suggested biosorption mechanism, Red and orange lines: electrostatic attractions, Green lines: BBR-Cd(II)-OTC complex interactions, blue lines: p-p stacking interactions

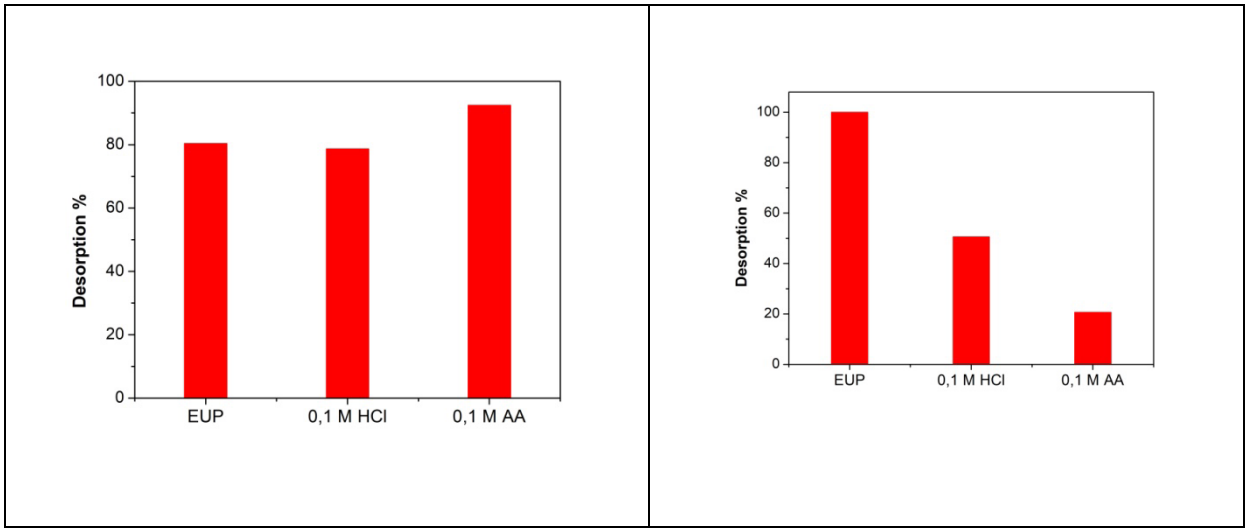

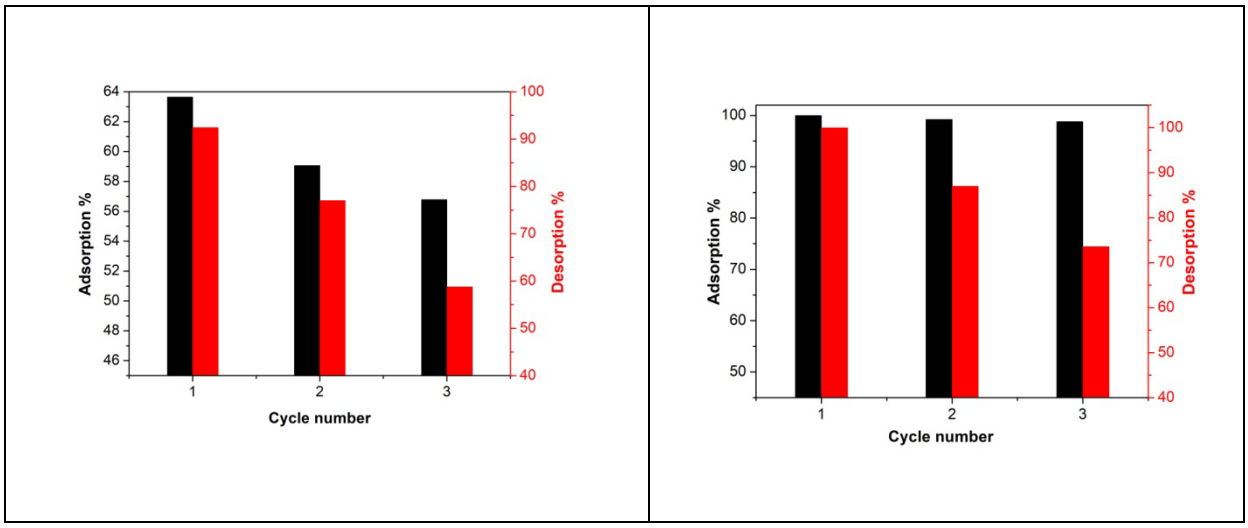

Fig. 10. Desorption studies of OTC and Cd(II) as function of **(a)** desorption time and **(b)** number of adsorption-desorption cycles

Table 1. The equations of used error functions.

Error Function	Definition	Eq N°	Description	References
Regression Coefficient	$R^2 = \frac{q_{e\,exp} - \overline{q_{e\,cal}}}{\sum[(q_{e\,exp} - \overline{q_{e\,cal}})^2 + (q_{e\,exp} - q_{e\,cal})^2]}$	3	$q_{e\,exp}$ and $q_{e\,cal}$ are the experimental and calculated sorption capacity (mg g^{-1}), respectively.	[1]
Chi-square test	$\chi^2 = (q_{e\,exp} - q_{e\,cal})^2/q_{e\,cal}$	4	n is the number of data points in the experiment.	[2]
Residual Sum of Squares	$RSS = \sum_{i=1}^{N}(y_{P,i} - y_{0,i})^2$ $RSS = \sum_{i=1}^{N}(q_{e\,cal} - q_{e\,exp})^2$	5	$y_{P,i}$ is the predicted value, $y_{0,i}$ is the experimental value.	[3]

Table 2. Experimental factors and levels in the CCD design.

Factor code	Factors	level			Star point (α = 2.3784)	
		Low (-1)	Central (0)	High (+1)	+α	-α
F_1	Adsorbent dosage (g L^{-1})	2	3	4	5.38	0.62
F_2	OTC concentration (μmol L^{-1})	175	225	275	343.92	106.08
F_3	Cd(II) concentration (μmol L^{-1})	400	600	800	1075.68	124.32
F_4	pH	4	6	8	10.75	1.24
F_5	Contact time (hour)	12	18	24	32.27	3.73

Table 3. The names and non-linear-forms of used kinetic models.

Kinetic model	Non linear form	Eq N°	Descriptions	References
BSf(n,α)	$q_{n,\alpha}(t) = q_e[1-(1+(n-1)(\frac{t}{\tau_{n,\alpha}})^{\alpha})^{\frac{-1}{n-1}}]$	8	$q_{n,\alpha}(t)$ and q_e are the adsorbed contaminant amounts (mg g^{-1}) at time t (min) and at equilibrium, respectively; n is the fractional reaction order; α is the fractal time index depending on the geometrical and energetic adsorbent heterogeneity; $\tau_{n,\alpha}$ is the characteristic time of the adsorption kinetics.	[4–7]
	$q_{n,\alpha}(t) = q_e[1-\mathrm{Exp}_n(-(\frac{t}{\tau_{n,\alpha}})^{\alpha})]$	9		
PFO=BSf(1,1)	$q(t) = q_{e,1}[1-\mathrm{Exp}(-\frac{t}{\tau_{1,1}})]$ $\tau_{1,1} = k_1^{-1}$	10	k_1 is the adsorption rate constant of the pseudo-first-order model (min^{-1}).	[7]
PSO=BSf(2,1)	$q(t) = q_{e,2}(\frac{\frac{t}{\tau_{2,1}}}{1+\frac{t}{\tau_{2,1}}})$ $\tau_{2,1} = (q_{e,2}k_2)^{-1}$	11	k_2 is the adsorption rate constant of the pseudo- second-order model (g mg^{-1} min^{-1}).	[7]
Weibull= BSf(1,α)	$q(t) = q_{e,W}[1-\mathrm{Exp}(-(\frac{t}{\tau_{1,\alpha}})^{\alpha})]$ $\tau_{1,\alpha} = k_{1,\alpha}^{-1}$	12	$k_{1,\alpha}$ is the adsorption rate constant of the Weibull model (min^{-1}).	[7]
Hill= BSf(2,α)	$q(t) = q_{e,H}(\frac{(\frac{t}{\tau_{2,\alpha}})^{\alpha}}{1+(\frac{t}{\tau_{2,\alpha}})^{\alpha}})$ $\tau_{2,\alpha} = (q_{e,H}k_{2,\alpha})^{-1}$	13	$k_{2,\alpha}$ is the adsorption rate constant of the Hill model (g mg^{-1} min^{-1}).	[7]
Brouers-Gaspard= BSf(1.5,α)	$q(t) = q_{e,BG}[1-(1+0.5(\frac{t}{\tau_{1.5,\alpha}})^{\alpha})^{-2}]$	14		[7]

Table 4. The names and non-linear-forms of used isotherm models.

Isotherm model	Non linear form	Eq N°	Descriptions	References
GBS	$q_{e,GBS} = q_{e,max}\left(1 - Exp_c\left[-\left(\frac{C_e}{b}\right)^a\right]\right)$	15	$q_{e,GBS}$ and $q_{e,max}$ are the adsorbed amount at equilibrium and the saturation adsorbed amount at equilibrium, respectively (mg g^{-1}). C_e is the adsorbate concentration in the liquid phase (mg L^{-1}). The coefficients (a) and (c) are related to the form, and (b) represents a scale parameter.	[7–9]
	$q_{e,GBS} = q_{e,max}\left(1 - \left[1+c\left(\frac{C_e}{b}\right)^a\right]^{\frac{-1}{c}}\right)$	16		
BS (c=0)	$q_{e,BS} = q_{e,maxBS}\left(1 - Exp\left[-\left(\frac{C_e}{b}\right)^a\right]\right)$	17	$q_{e,maxBS}$ is the maximum adsorption capacity for the BS model.	[7]
Freundlich (c=0 and $C_e \ll b$)	$q_{e,F} = k_F C_e^a$	18	k_F is the Freundlich constant, indicating the adsorption capacity.	[7]
Jovanovich (c=0 and a=1)	$q_{e,J} = q_{e,maxJ}\left(1 - Exp\left[-\frac{C_e}{b}\right]\right)$	19	$q_{e,maxJ}$ is the maximum adsorption capacity for the Jovanovich model.	[7]
HS (c=1)	$q_{e,HS} = q_{e,maxHS}\left(1 - \left[1+\left(\frac{C_e}{b}\right)^a\right]^{-1}\right)$	20	$q_{e,maxHS}$ is the maximum adsorption capacity for the HS model.	[7]
Langmuir (c=1 and a=1)	$q_{e,L} = q_{e,maxL}\left(\frac{C_e/b}{1 + C_e/b}\right)$	21	$q_{e,maxL}$ is the maximum adsorption capacity for the Langmuir model.	[7]
BG (c=0.5)	$q_{e,BG} = q_{e,maxBG}\left(1 - Exp_{c=0.5}\left[-\left(\frac{C_e}{b}\right)^a\right]\right)$	22	$q_{e,maxBG}$ is the maximum adsorption capacity for the BG model.	[7]
	$q_{e,BG} = q_{e,maxBG}\left(1 - \left[1+\frac{1}{2}\left(\frac{C_e}{b}\right)^a\right]^{-2}\right)$			

Table 5. Model summary

	OTC	Cd(II)
R-squared (R^2)	0.96056	0.97598
Adjusted R-squared	0.91753	0.94978
MS Residual	18.36288	26.07838

Table 6. Thermodynamic parameters for the biosorption of OTC and Cd(II) onto BBR from binary systems at various temperatures (F_1 = 4.1892 g/L ; F_2 = 165.54 µM ; F_3 = 362.16 µM ; F_4 = 6 ; F_5 = 25.135 h).

Contaminant	T (°K)	K_d	ΔH^0 (kJ mol^{-1})	ΔS^0 (J/mol.K)	ΔG^0 (kJ mol^{-1})
OTC	293.15	0.42	22.76	70.28	-43.37
	303.15	0.55			-44.07
	313.15	0.75			-44.77
	323.15	0.99			-45.48
Cd(II)	293.15	24289.74	35.72	204.94	-95.80
	303.15	32386.40			-97.85
	313.15	48579.70			-99.90
	323.15	97159.66			-101.94

References

[1] S.L. Chan, Y.P. Tan, A.H. Abdullah, S.T. Ong, Equilibrium, kinetic and thermodynamic studies of a new potential biosorbent for the removal of Basic Blue 3 and Congo Red dyes: Pineapple (Ananas comosus) plant stem, Journal of the Taiwan Institute of Chemical Engineers. 61 (2015) 306–315. doi:10.1016/j.jtice.2016.01.010.

[2] E. Sharifpour, H. Haddadi, M. Ghaedi, Optimization of simultaneous ultrasound assisted toxic dyes adsorption conditions from single and multi-components using central composite design: Application of derivative spectrophotometry and evaluation of the kinetics and isotherms, Ultrasonics Sonochemistry. 36 (2017) 236–245. doi:10.1016/j.ultsonch.2016.11.011.

[3] P. Janoš, Biosorption of Synthetic Dyes on Spruce Wood\r\nShavings from Binary Solutions: A Comparison\r\nof Equilibrium Models, American Chemical Science Journal. 4 (2014) 638–656. http://www.sciencedomain.org/abstract.php?iid=475&id=16&aid=4322#.VMWGk0SFUJJ.mendeley.

[4] T.J. Al-Musawi, F. Brouers, M. Zarrabi, Kinetic modeling of antibiotic adsorption onto different nanomaterials using the Brouers–Sotolongo fractal equation, Environmental Science and Pollution Research. 24 (2017) 4048–4057. doi:10.1007/s11356-016-8182-z.

[5] F. Brouers, O. Sotolongo-Costa, Generalized fractal kinetics in complex systems (application to biophysics and biotechnology), Physica A: Statistical Mechanics and Its Applications. 368 (2006) 165–175. doi:10.1016/j.physa.2005.12.062.

[6] S.M. Miraboutalebi, S.K. Nikouzad, M. Peydayesh, N. Allahgholi, L. Vafajoo, G. McKay, Methylene blue adsorption via maize silk powder: Kinetic, equilibrium, thermodynamic studies and residual error analysis, Process Safety and Environmental Protection. 106 (2017) 191–202. doi:10.1016/j.psep.2017.01.010.

[7] S. Karoui, R. Ben Arfi, K. Mougin, A. Ghorbal, A.A. Assadi, A. Amrane, Synthesis of novel biocomposite powder for simultaneous removal of hazardous ciprofloxacin and methylene blue : Central composite design , kinetic and isotherm studies using Brouer-Sotolongo family models, Journal of Hazardous Materials. (2019) 121675.

[8] F. Brouers, Statistical Foundation of Empirical Isotherms, Open Journal of Statistics.

04 (2014) 687–701. doi:10.4236/ojs.2014.49064.

[9] F. Brouers, F. Marquez-Montesino, Dubinin isotherms versus the Brouers–Sotolongo family isotherms: A case study, Adsorption Science and Technology. 34 (2016) 552–564. doi:10.1177/0263617416670909.